

Competing orders and quantum criticality in doped antiferromagnets

Matthias Vojta, Ying Zhang, and Subir Sachdev

Department of Physics, Yale University, P.O. Box 208120, New Haven, CT 06520-8120, USA

(March 10, 2000; cond-mat/0003163)

We use a number of large- N limits to explore the competition between ground states of square lattice doped antiferromagnets which break electromagnetic $U(1)$, time-reversal, or square lattice space group symmetries. Among the states we find are d -, $(s^* + id)$ -, and $(d_{x^2-y^2} + id_{xy})$ -wave superconductors, Wigner crystals, Wigner crystals of hole pairs, orbital antiferromagnets (or staggered-flux states), and states with spin-Peierls and bond-centered charge stripe order. In the vicinity of second-order quantum phase transitions between the states, we go beyond the large- N limit by identifying the universal quantum field theories for the critical points, and computing the finite temperature, quantum-critical damping of fermion spectral functions. We identify candidate critical points for the recently observed quantum-critical behavior in photoemission experiments on $\text{Bi}_2\text{Sr}_2\text{CaCu}_2\text{O}_{8+\delta}$ by Valla *et al.* (Science **285**, 2110 (1999)). These involve onset of a charge density wave, or of broken time-reversal symmetry with $d_{x^2-y^2} + id_{xy}$ or $s^* + id$ pairing, in a d -wave superconductor. It is not required (although it is allowed) that the stable state in the doped cuprates to be anything other than the d -wave superconductor—the other states need only be stable nearby in parameter space. At finite temperatures, fluctuations associated with these nearby states lead to the observed fermion damping in the vicinity of the nodal points in the Brillouin zone. The cases with broken time-reversal symmetry are appealing because the order parameter is not required to satisfy any special commensurability conditions. The observed absence of inelastic damping of quasiparticles with momenta (π, k) , (k, π) (with $0 \leq k \leq \pi$) also appears very naturally for the case of fluctuations to $d_{x^2-y^2} + id_{xy}$ order.

Contents	
I	Introduction 1
A	Quantum phase transitions 4
II	$\text{Sp}(2N)$ t-J model in the large-N limit 6
A	Ground states at $N = \infty$ 8
1	Homogeneous superconductor 8
2	Spin-Peierls state 9
3	States with stripe charge order 9
4	Wigner crystals of Cooper pairs 11
5	Wigner crystals of single charges 12
B	Influence of additional model parameters 12
1	Longer-range hopping 12
2	Biquadratic exchange 12
3	Next-nearest neighbor exchange 13
4	Alternative interaction decoupling 14
C	Phase transitions at $N = \infty$ 15
III	Continuous quantum phase transitions 16
A	d -wave to $(s^* + id)$ -wave or $(d_{x^2-y^2} + id_{xy})$ -wave 16
1	Unequal velocities 18
2	$T > 0$ spectral functions 18
B	\mathcal{C} symmetry breaking in a d -wave superconductor 20
C	OAF order in a d -wave superconductor 21
IV	Discussion 21
APPENDIXES 24	

A Perturbation theory for fermion damping 24

I. INTRODUCTION

A minimal approach to the physics of the cuprate superconductors is to assume that all relevant ground states can be completely characterized by the manner in which they break the global symmetries of the underlying Hamiltonian. Related ideas have been discussed by others in Refs. 1–3; for a review by one of us see Ref. 4, and for early work we shall extend in this paper see Ref. 5. The global symmetries are:

(i) \mathcal{S} - the electromagnetic $U(1)$ symmetry, which is broken by the appearance of superconducting order;
(ii) \mathcal{M} - the $SU(2)$ spin rotation invariance symmetry, which is broken by magnetically ordered states like the Néel state;

(iii) \mathcal{C} - the space group of the square lattice, which we will consider broken when an observable invariant under \mathcal{S} and \mathcal{M} , like site or bond-charge density, is not invariant under space group transformations; and
(iv) \mathcal{T} - time-reversal symmetry.

Even in this limited approach, a surprisingly rich number of phases and phase transitions are possible. While at low enough temperatures, every phase is amenable to a conventional quasiparticle-like description, anomalous behavior can appear in the vicinity of second-order quantum critical points between the phases.

This paper will study the competition between phases

which break one or more of \mathcal{S} , \mathcal{C} , and \mathcal{T} symmetries, and describe the universal theories of the associated quantum critical points. We will do this in the context of a number of large- N computations which, by construction, only produce ground states in which \mathcal{M} symmetry is preserved. Transitions at which \mathcal{M} symmetry is broken are quite important for certain aspects of the physics of the cuprates (as we shall discuss later in this section), and the absence of explicit computations for where such transitions may occur is the primary limitation of our approach.

A brief discussion of mainly the large- N results has appeared in an earlier paper⁶.

A global perspective on our approach is provided by the schematic phase diagram in Fig. 1 (see also the discussion by Zaanen¹ on related phases). This sketches the qualitative evolution of the physics as a function of the hole doping, δ , and N , the size of the symmetry group of spin rotations, \mathcal{M} : we will primarily consider models in which this symmetry group is generalized from $SU(2)$ to $Sp(2N)$ (specific details in Section II).

Let us first discuss the physics at $\delta = 0$ as a function of N . For small N , including the physical case, $N = 1$, we know that the ground state has magnetic Néel order, and so breaks \mathcal{M} symmetry. This symmetry is restored by a continuous quantum phase transition at the point X . Above X , it is believed that one enters a paramagnetic phase which generically has ‘Peierls’ order^{7–9,5,10,11}: in such a state all sites are equivalent, but the charge and energy densities on the bonds¹² have the modulation indicated schematically by the pattern in Fig. 1. It is evident that such a state breaks only a \mathcal{C} symmetry. So the \mathcal{M} and \mathcal{C} symmetries vanish at the common point X , a phenomenon not generically expected in a Landau theory-like approach suitable for high dimensions, but possible in the present low-dimensional system with strong quantum fluctuations¹³. Further above the point X , other phases like the ‘orbital antiferromagnet’^{14–18} (to be described shortly) are also possible in certain models and we will also discuss these.

The primary purpose of this paper is to study the physics for $\delta > 0$. Ideally, we should do this along the path A_2 in Fig. 1, which meets the $\delta = 0$ line below X . Instead, we will offer a controlled, quantitative theory along the path A_1 which meets the $\delta = 0$ line above X . The implicit assumption underlying such a strategy is that the quantum critical point X is “close” to the regime of physically relevant parameters. Then we can expect that the phases with \mathcal{M} symmetry preserved along the path A_1 are related to the phases with \mathcal{M} symmetry preserved accessed by increasing δ along the path A_2 .

This paper describes the intricate interplay between \mathcal{C} , \mathcal{S} , and \mathcal{T} symmetry breaking along A_1 : the body of the paper contains a large number of phase diagrams as a function of δ and a dimensionless measure of the strength of the long-range Coulomb interactions, and all of these lie along A_1 . Over a significant regime of parameters, we find that \mathcal{C} symmetry is broken at smaller values of δ ;

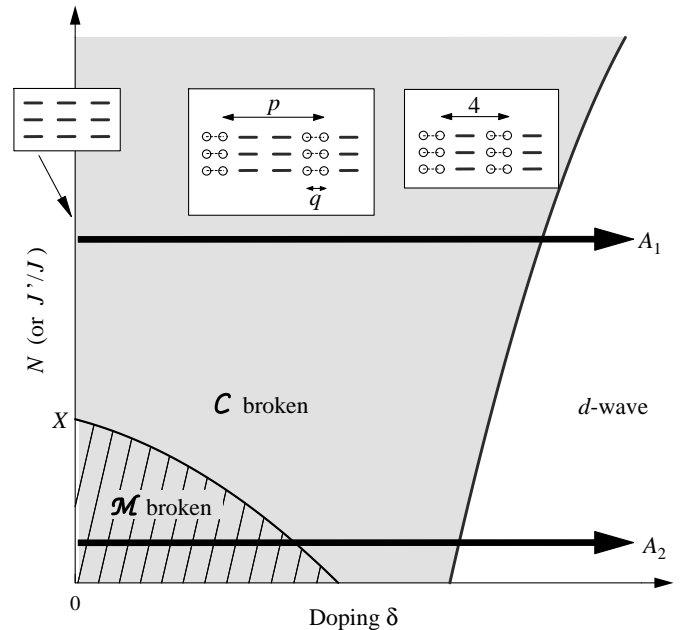


FIG. 1. Schematic phase diagram of doped antiferromagnets. See Section I for further general discussion and Section II for specific quantitative phase diagrams along the line A_1 . The vertical axis represents the size, N , of the symmetry group of spin rotations, \mathcal{M} . Although this parameter is not experimentally variable, we propose that a similar phase diagram would be obtained as a function of the ratio of the second (J') to first (J) neighbor exchange interactions. There is evidence^{7–9,5,10,11} that the Peierls order shown above X at $\delta = 0$ is also found in $J' - J$ antiferromagnets. The magnetic \mathcal{M} symmetry is broken in the hatched region, while \mathcal{C} symmetry is broken in the shaded region; there are numerous additional phase transitions at which the detailed nature of the \mathcal{M} or \mathcal{C} symmetry breaking changes - these are not shown. For $\delta = 0$, \mathcal{M} symmetry is broken only below the critical point X , while \mathcal{C} symmetry is broken only above X . Over a significant parameter regime, and for not too small δ , the \mathcal{C} symmetry breaking appears in the stripe patterns shown, with accompanying anisotropic superconductivity which breaks \mathcal{S} . For some other parameter regimes (as in Fig 11), the \mathcal{C} symmetry breaking is realized by orbital antiferromagnetic (or staggered flux) order: such \mathcal{C} symmetry breaking cannot survive all the way down to the point X . The superconductivity is pure d -wave only in the large δ region where \mathcal{C} and \mathcal{M} are not broken. The smaller δ region of the superconductor which preserves \mathcal{C} and \mathcal{M} can also exhibit $(d_{x^2-y^2} + id_{xy})$ - or $(s^* + id)$ -wave superconductivity.

for very small values of δ , the \mathcal{C} -broken phase is an insulating Wigner crystal-like state, but for larger δ we obtain a state with co-existing^{1,19} stripe charge order^{20–22} and superconductivity, as sketched in Fig. 1. Moving to smaller values of N in Fig. 1, we expect a transition to a state with \mathcal{M} symmetry broken which is not contained in our computations here. The magnetic order appears in a background of charge stripe order that is present on both sides of the transition, and the spin

polarization is therefore expected to be incommensurate and *collinear*². It is important to contrast this magnetic order from the incommensurate “spiral” states that were considered some time ago²³: such states have coplanar spins and do not require co-existing charge order. In contrast, the incommensurate, collinear spin states must coexist with charge stripe order²⁴, and there is evidence that the spin incommensuration observed experimentally is indeed of this type^{25–27}. Stripe charge order has been discussed first in the context of mean-field theories for the Hubbard model^{20–22}, a brief comparison of these results with the present theory will be given in Sec. II A 3.

The order parameter for the collinear spin ordering, discussed above, is an ordinary $O(3)$ vector^{24,28,29}, identical to that for the transition at the point X at $\delta = 0$. To understand the transition at which \mathcal{M} symmetry is restored at $\delta > 0$, we need to explore the possibility of the magnetic order parameter coupling to gapless fermion excitations. In all our charge stripe states, we find a strong pairing tendency between the holes, and as a consequence, the fermion excitation spectrum is either fully gapped, or has gapless excitations only at special points in the Brillouin zone. Assuming that momentum conservation prohibits the coupling between the magnetic order parameter and the gapless fermion excitations (if present), we arrive at the conclusion that the spin disordering transition at $\delta > 0$ is in precisely the same universality class as that at X . Fig. 1 contains a line, emerging from the point X , along which a transition to \mathcal{M} symmetry restoration takes place. The gist of our arguments above is that the universality class of the transition all along this line is likely to be identical to that at X . The implications for such a scenario for experiments (especially NMR³⁰) has been reviewed recently in Ref. 4. A related scenario, and quantitative comparisons with experiments, has been provided recently by Morr *et al.*³¹.

Returning to the physics along A_1 , we briefly catalog the properties of the states found. Further details appear in Section II, but the reader is urged to glance at the phase diagrams in Figs 3-11 at this stage. It is also worth noting explicitly here that all of these phase diagrams were obtained in the large N limit, and the precise numerical values of the parameters at the phase boundaries are not expected to be accurate for $SU(2)$: nevertheless, the general topology of the phase diagrams, and the trends in stability between the various phases, are expected to be realistic.

(i) Superconductors with \mathcal{C} symmetry: These appear for large δ , and for a large region of parameters the Cooper pairs are in a d -wave state. We also find a $(s^* + id)$ -wave state^{32,5} a $(d_{x^2-y^2} + id_{xy})$ -wave state^{33,34}, both of which break \mathcal{T} symmetry, but preserve \mathcal{C} symmetry; the latter state has a non-vanishing spin Hall conductance³⁵.

(ii) Spin-Peierls: An insulating spin-Peierls state at $\delta = 0$ was discussed above: it breaks only \mathcal{C} symmetry. We also obtained⁵ for a range of $\delta > 0$ a superconducting state with precisely the same pattern of \mathcal{C} symmetry breaking; naturally, \mathcal{S} is also broken in such a state. The

signature of both states in neutron scattering would be the same: all sites are equivalent, but there is a modulation in the energy and charge densities on the bonds with a period of 2 lattice spacings.

(iii) Stripes: The striped states are similar to the superconducting spin-Peierls states above, but all sites are no longer equivalent. The states have a $p \times 1$ unit cell and the holes are concentrated on a strip of width q ; both p and q were always found to be even. The width q regions form strong one-dimensional superconductors (Luther-Emery liquids), and coupling between these hole-rich regions leads to anisotropic superconductivity. The hole pairing also always prefers stripes in a *bond-centered* configuration^{36,6}: the ground state possesses a reflection symmetry about the centers of certain columns on bonds, but not about any column of sites. Distinguishing² bond- and site-centering^{20–22} is an important issue to be resolved by future experiments.

(iv) Wigner crystal: An insulating state for $\delta > 0$ is the familiar Wigner crystal of holes, which breaks only \mathcal{C} symmetry. This state appears when the strength of the Coulomb interactions is large enough.

(v) Pair crystal: An alternative insulating state can appear at small $\delta > 0$ and weaker Coulomb interactions. The exchange interactions induce pairing of holes, and the resulting composites then form a Wigner crystal to minimize the Coulomb repulsion. The underlying square lattice can induce strong distortions on the usual triangular structure of the Wigner crystal, so that the state can look like a striped configuration with an additional longitudinal charge modulation along each hole-rich stripe.

(vi) Orbital antiferromagnet: This also known as the “staggered flux” state^{14–18}. There are staggered, circulating currents around each square lattice plaquette, and the state breaks \mathcal{T} symmetry. The unit cell has two sites and so \mathcal{C} symmetry is also broken, but a combination of translation by one site and time-reversal remains unbroken. At half-filling, this state has gapless fermionic excitations at nodal points along the diagonals of the Brillouin zone, like the d -wave superconductor. The state with co-existing orbital antiferromagnetism and d -wave superconductivity has broken \mathcal{C} symmetry (the unit cell has 2 sites) and is distinct from the $(s^* + id)$ -wave or $(d_{x^2-y^2} + id_{xy})$ -wave superconductor.

The competition between \mathcal{C} , \mathcal{M} and \mathcal{S} breaking leading to phases with co-existing orders (as in (ii) and (iii) above) has been discussed by Zaanen¹ on phenomenological grounds. However, he focuses mainly on the bosonic order parameters, while fermionic excitations will play an important role in our considerations.

Phases related to those in (i), (iii), (iv) and (v), and associated phase diagrams, appear in the work of Kivelson, Fradkin and Emery¹⁹. These authors use liquid-crystal like pictures, in which quasi-independent one-dimensional Luttinger liquids are allowed to fluctuate transversely, and obtain qualitative phase diagrams. In contrast, our work is intrinsically two-dimensional, and

the quantum fluctuations are tied more strongly to the underlying lattice sites; further we shall obtain quantitative results for phase diagrams, albeit in a large N limit.

It is interesting that none of the states above is an ordinary Fermi liquid: such a state appears to be always unstable to some ordering induced by breaking one or more of \mathcal{C} , \mathcal{S} , \mathcal{M} , or \mathcal{T} symmetries. In this respect our results are similar to recent results of Honerkamp *et al.*³⁷ and Ledermann *et al.*³⁸; however, they find renormalization group instabilities of the Fermi liquid to states somewhat different from those discussed above.

We conclude our discussion of mean-field theory by noting that a separate study of \mathcal{C} symmetry breaking in doped antiferromagnets has been carried out recently by Stojković *et al.*³⁹: they examined the competition between stripe and Wigner crystal-like phases in a semi-classical theory of hole dynamics.

A. Quantum phase transitions

We have already discussed above the nature of the \mathcal{M} ordering transition in Fig. 1, and its possible relationship to NMR experiments^{4,30}. Here we shall explore the nature of the quantum phase transitions between the phases found along A_1 (which do not involve order parameters associated with \mathcal{M} symmetry), and their possible relationship to quantum critical scaling observed in a recent photoemission experiment⁴⁰.

Many of the transitions in our phase diagrams are first order. These do not have interesting fluctuation spectra, and we will not consider them further. We will consider second order transitions at $\delta > 0$, in which the ground state is superconducting on both sides of the transitions (see Fig 2). One of these states is a d -wave superconductor, while the other is denoted as superconducting state X in Fig 2; we will discuss different candidates for state X below. Such second order transitions fall into two classes depending on the behavior of the fermion spectra in the vicinity of the nodal points of the d -wave superconductor. These points are at⁴⁰ $(\pm K, \pm K)$ with $K = 0.391\pi$ (at optimal doping), and throughout the remainder of this paper, unless noted otherwise, we will be implicitly referring to the fermionic Bogoliubov quasiparticles in the vicinity of these points. (We will discuss the properties of the gapped fermionic quasiparticles near $(0, \pi)$, $(\pi, 0)$ at the end of Section I.) The two classes are:

(A) There is efficient scattering and damping of the nodal fermionic quasiparticles, and as a result the fermionic spectral function obeys ‘naive’ quantum critical scaling (see (1.1) below), of the type observed experimentally⁴⁰.
(B) the gapless, Bogoliubov, fermionic quasiparticles can be neglected in the scaling limit of the critical theory, and so their damping appears only upon considering corrections to scaling, and vanishes with a super-linear powers of temperature (T) as $T \rightarrow 0$.

The simplest of the transitions in class A are those that

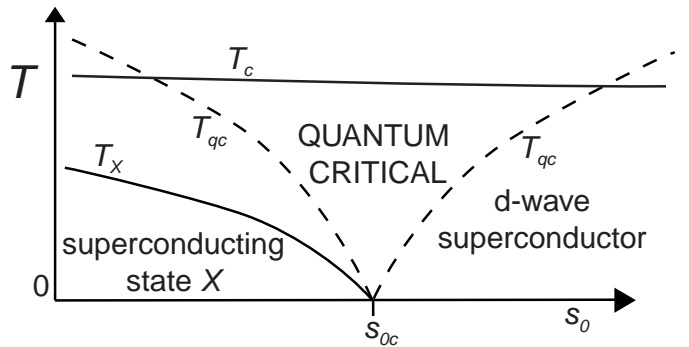


FIG. 2. Finite temperature (T) phase diagram in the vicinity of a second order quantum phase transition from a d -wave superconductor as a function of some parameter in the Hamiltonian, s_0 (which is possibly, but not necessarily, the hole concentration δ). Superconductivity is present at temperatures below T_c , and the superfluid density is non-zero on both sides of s_{0c} . The state X is characterized by some other order parameter (in addition to superconductivity) which vanishes above a temperature T_X . We will consider a number of possibilities for the state X in this paper, including broken \mathcal{T} symmetry in a $(s^* + id)$ -wave or a $(d_{x^2-y^2} + id_{xy})$ -wave superconductor, or in an orbital antiferromagnet, and states with broken \mathcal{C} symmetry with charge density wave order. Of particular interest will be transitions for which the scaling form (1.1) applies to the nodal quasiparticles in the quantum critical region $T > T_{qc}$. As we discuss in Section I A, this scaling could continue to apply even above T_c provided the thermal length associated with proximity to the quantum phase transition at $s = s_{0c}$ remains smaller than the phase coherence length. It is the proposal of this paper that the high-temperature superconductor studied in the experiments of Ref 40 is in the vicinity of s_{0c} . Indeed, this system could have $s_0 > s_{0c}$, so that the ultimate ground state is an ordinary d -wave superconductor—the fermion spectrum then exhibits consequences of fluctuations into state X at $T > T_{qc}$.

involve time-reversal symmetry breaking in the d -wave superconductor: transitions from a d -wave superconductor to a state X which is either a $(s^* + id)$ -wave^{32,5} or a $(d_{x^2-y^2} + id_{xy})$ -wave^{33,34} superconductor. It is important to note that both these transitions occur for only at a *finite* attractive coupling in the s^* or d_{xy} pairing channels. This is to be contrasted to pairing instabilities of a Fermi liquid, which would occur at infinitesimal attraction in either channel. However, when the parent state is a $d_{x^2-y^2}$ -wave superconductor, the vanishing density of states at the Fermi level removes the usual BCS log divergence in the Cooper pair propagator, and a finite attraction is required for further pairing in the s^* or d_{xy} channels. This finite coupling instability is directly responsible for a non-trivial quantum critical point, with strong thermal and quantum fluctuations leading to class A behavior, whose effects we shall describe and exploit in this paper. Much of the more recent discussion (see Ref. 41 and references therein) of $(d_{x^2-y^2} + id_{xy})$ -wave superconductivity has focused on the case where this or-

der is induced by external perturbations like an applied magnetic field, and is motivated partly by the experiments of Ref. 42. In contrast, in our paper, we are interested in the spontaneous appearance of such order, and this is necessarily associated with a sharp transition and \mathcal{T} symmetry breaking. There is a divergent susceptibility associated with this symmetry breaking, and this will lead to a low energy amplitude fluctuation mode distinct from that discussed in Ref. 41.

Another transition involving breaking of time-reversal symmetry is that between a d -wave superconductor and a state X in which d -wave superconductivity and orbital antiferromagnetism coexist. Unlike the above, this transition will be shown to be in class B.

A slightly more complicated transition in class A is one in which X involves the onset of \mathcal{C} symmetry breaking in a d -wave superconductor: such a transition is the boundary of the \mathcal{C} -broken region in Fig. 1. However, a special condition is required for such a transition to be in class A: the charge-ordering wavevector should precisely equal the wavevector between two nodal points in the d -wave superconductor; otherwise the transition is in class B. The theory for such a transition is closely related to models for the onset of antiferromagnetism in a d -wave superconductor considered recently by Balents *et al.*⁴³. We note that others have also discussed quantum phase transitions involving stripe or charge density wave order in the cuprate superconductors in recent years^{1,44}; however, in contrast to us, these works have either ignored interplay with the dynamic properties of the fermions¹, or focused on transitions in a Fermi liquid ground state⁴⁴, not a d -wave superconductor.

The hallmark of the class A transition is that in its $T > 0$ “quantum-critical” region¹³ (see Fig 2), the fermion Green’s function near one of the nodal points of the d -wave superconductor obeys

$$G_f(k, \omega) = \frac{\mathcal{A}_f}{T^{(1-\eta_f)/z}} \Phi_f \left(\frac{\hbar\omega}{k_B T}, \frac{vk}{(k_B T)^{1/z}} \right); \quad (1.1)$$

here z is the dynamic critical exponent ($z = 1$ for the specific models solved in this paper), k measures the distance from one of the nodal points of the d -wave superconductor, ω is a measuring frequency, v is a velocity (for $z = 1$), \mathcal{A} is an overall amplitude, η_f is a universal anomalous dimension, and Φ_f is a universal scaling function of its two arguments. We emphasize that unless the system happens to be precisely at the quantum-critical point, which is generically not expected to be the case, the scaling form (1.1) will eventually fail as $T \rightarrow 0$. Indeed, if define a lower crossover temperature T_{qc} so that (1.1) holds for $T > T_{qc}$, then $T_{qc} \sim |s_0 - s_{0c}|^{z\nu}$ where s_0 is some coupling constant in the Hamiltonian, the $T = 0$ quantum critical point is at $s_0 = s_{0c}$, and ν is the usual correlation length critical exponent. For $T < T_{qc}$, normal Bogoliubov quasiparticle behavior emerges, and this is indeed observed^{40,45–49} to be the case experimentally at very low T . We emphasize further that it is not even

necessary that the point $s_0 = s_{0c}$ be in an experimentally accessible parameter regime. So if we are considering the d -wave to $(d_{x^2-y^2} + id_{xy})$ -wave transition (for definiteness), then it is not required (although it is permissible) that the true ground state of a cuprate compound be a $(d_{x^2-y^2} + id_{xy})$ -wave superconductor over some doping regime. It is only necessary that a $(d_{x^2-y^2} + id_{xy})$ -wave superconductor be close enough to the physical regime, so that dynamic fluctuations to $(d_{x^2-y^2} + id_{xy})$ -wave order are apparent in the quantum-critical regime. Postulating the existence of a $(d_{x^2-y^2} + id_{xy})$ -wave ground state somewhere in parameter space is then a powerful theoretical tool for obtaining a controlled description of this intermediate temperature regime. When this paper was almost complete, new experimental evidence for broken \mathcal{T} symmetry near defects was reported⁵⁰; these results support the hypothesis that the bulk energy of a superconductor with broken \mathcal{T} symmetry is not very much higher than that of a d -wave superconductor⁵¹, and that a quantum phase transition between these states may indeed be near the experimentally accessible parameter space.

One of the purposes of this paper is to develop a method for computing the universal function Φ_f in (1.1) for the various transitions in class A noted above. We will find that two different methods are necessary, depending on the frequency/wavevector regime being accessed. For $vk \gg k_B T$ or $\hbar\omega \gg k_B T$, a straightforward resummation of a renormalized perturbative expansion suffices. However, for $vk < k_B T$ and $\hbar\omega < k_B T$, an entirely different approach has to be developed. Now there is strong damping induced by scattering between thermally induced excitations, and we compute it in a self-consistent theory of excitations scattering via a renormalized, temperature dependent T -matrix.

It is important to keep in mind that the class A transitions being considered here have long-range superconducting order on both sides of the quantum critical point. The order parameter associated with the transition involves either \mathcal{C} or \mathcal{T} symmetry breaking, and has no direct relationship to \mathcal{S} symmetry. The main role of the superconducting order is to define the bare spectrum of the fermion excitations which then interact with the critical order parameter fluctuations. In the experiments⁴⁰, scaling related to (1.1) is also observed above the superconducting transition temperature, T_c (which is quite distinct from T_{qc} and could be either above or below it); indeed there is no signature of T_c in the photoemission spectrum (while below T_{qc} there is a crossover to conventional quasiparticle behavior). Our quantum-critical theory entirely neglects the fluctuations of the superconducting order itself, but this does not limit its applicability to below T_c ; rather, we only need to impose the more limited constraint that the phase coherence length of the superconducting order parameter is larger than the inelastic scattering length of the class A transition with \mathcal{C} or \mathcal{T} symmetry breaking. This constraint is automatically satisfied below T_c , and can easily be satisfied over a wide range of temperatures above T_c . Indeed, the lat-

ter length, by (1.1), decreases as $\sim 1/T^{1/z}$, and so the constraint becomes less stringent as T increases.

Finally, we discuss the important issue of the gapped quasiparticles well away from the nodal points of the d -wave superconductor. The fermionic quasiparticles with momenta (π, k) , (k, π) (with $0 \leq k \leq \pi$) have a non-zero excitation energy which is a minimum near^{48,49} $k \approx 0.18\pi$ at optimal doping. Experiments^{45–47} clearly indicate that these quasiparticles are sharply defined at all temperatures below T_c , and do not show any sign of “quantum-critical” damping (we thank M. Norman and M. Randeria for emphasizing this to us). So the order parameter fluctuations discussed above, which are responsible for the quantum-critical damping near the nodal points $(\pm K, \pm K)$, clearly cannot couple efficiently to the quasiparticles on the lines between (π, π) and $(\pi, 0)$, $(0, \pi)$. For the case of a transition from d -wave to $(d_{x^2-y^2} + id_{xy})$ -wave superconductivity (discussed in Section III A) this is, in fact, very naturally the case: the d_{xy} order parameter $\sim \sin k_x \sin k_y$ vanishes when either $k_x = \pi$ or $k_y = \pi$. For the transition from d -wave to $(s^* + id)$ -wave (also discussed in Section III A), the s^* order parameter $\sim (\cos k_x + \cos k_y)$, and this vanishes at the points $(\pi, 0)$, $(0, \pi)$; however there will be some residual coupling as one moves away from these points to (π, k) , (k, π) with $k \approx 0.18\pi$. Finally, for the transitions in class A involving the onset of \mathcal{C} symmetry breaking (to be discussed in Section III B), momentum conservation makes the coupling of the order parameter to fermions near $(\pi, 0)$, $(0, \pi)$ very ineffective: the order parameter scatters the fermions to a region of the Brillouin zone where the quasiparticles have an even higher energy.

The outline of the remainder of this paper is as follows. In Section II we present the results of the large- N study along A_1 . The universal theories of the second-order quantum phase transitions appear in Section III. A summary of our results and a discussion of experimental issues is in Section IV. A calculation of the fermion damping in a naive renormalized perturbation theory, and its failure in the low frequency regime $\hbar\omega < k_B T$ is discussed in Appendix A. Readers not interested in specific details of our results can glance at Figs 3-11 and move ahead to Section IV.

II. Sp(2N) t -J MODEL IN THE LARGE- N LIMIT

For a microscopic investigation of the ground states of doped antiferromagnets we start from the usual $t - J$ model \mathcal{H}_{tJ} on the sites i of a square lattice, which is complemented by a Coulomb \mathcal{H}_V interaction between the electrons, $\mathcal{H} = \mathcal{H}_{tJ} + \mathcal{H}_V$,

$$\begin{aligned} \mathcal{H}_{tJ} &= \sum_{i>j} \left[-t_{ij} c_{i\sigma}^\dagger c_{j\sigma} + \text{H.c.} + J_{ij} \left(\mathbf{S}_i \cdot \mathbf{S}_j - \frac{n_i n_j}{4} \right) \right], \\ \mathcal{H}_V &= \sum_{i>j} V_{ij} n_i n_j. \end{aligned} \quad (2.1)$$

The electron operators c^\dagger exclude double occupancies which expresses the (infinite) electronic on-site repulsion. $n_i = c_{i\sigma}^\dagger c_{i\sigma}$ is the charge density at site i . We will primarily be concerned with the case where the fermion hopping, t_{ij} , and exchange, J_{ij} , act only when i, j are nearest neighbors, in which case $t_{ij} = t$ and $J_{ij} = J$; however, we will occasionally refer to cases with second neighbor hopping (t') or exchange (J'). For the off-site Coulomb repulsion V_{ij} we assume weak or no screening since the zero-temperature ground states will be either insulating or superconducting; in both cases the density of states at the Fermi level vanishes. Therefore we will use a $1/R$ decay of the interaction, $V_{ij} = V/|\mathbf{R}_i - \mathbf{R}_j|$, and the strength of the repulsion is parameterized by V . The V_{ij} are included to counter-act the phase separation tendency of the $t - J$ model^{52,53–55}, and play a key role in our analysis.

We shall be interested in describing the ground state of \mathcal{H} as a function of its couplings and the average doping concentration δ . We generalize the spin symmetry^{9,5,56} from SU(2) to Sp(2N) and examine the limit of large degeneracy N . In the large- N approach the ground state of the system can be found in a saddle-point approximation (which becomes exact for $N = \infty$). Large- N expansions have been applied to a large number of antiferromagnetic spin systems as well as to models with doping. The motivation for using the symplectic Sp(2N) generalization instead of the more common SU(N) variant is that it does not rely on a two-sublattice structure of the underlying antiferromagnet and is therefore more appropriate for systems where frustration may play a role⁹. Furthermore, the Sp(2N) approach includes naturally pairing of spins which leads to superconducting ground states when the system is doped. (Note that both Sp(2N) and SU(2N) reduce to the usual SU(2) symmetry group for $N = 1$.) Apart from studies of t - J models like (2.1), Hubbard models with Sp(2N) symmetry have also been studied^{57,58}.

The behavior of the system in the large- N limit depends on the representation of Sp(2N) used for the spin operators. In the context of SU(N) approaches to the 2D Heisenberg model especially totally symmetric (bosonic) and totally antisymmetric (fermionic) representations have been applied, see e.g. Refs. 14,16,59,60. For the present problem of the $t - J$ model it turns out that a simple large- N limit (leading to a saddle point in the free-energy functional) exists only for a fermionic representation of the spin degrees of freedom. As discussed in the introduction, in this case the ground state of the undoped (Heisenberg) model does not break spin rotation symmetry \mathcal{M} . Instead, translation and rotation symmetries \mathcal{C} are broken and the state has been shown to be a paramagnetic spin-Peierls state which can also be considered as a *bond-centered* charge density wave. Recent work¹⁰ has shown strong evidence for this order in the *frustrated* SU(2) quantum antiferromagnet on a square lattice (with $J' > 0$).

Let us now describe the details of the large- N approach. In the following we consider spins transforming under the antisymmetric product of m fundamentals of $\text{Sp}(2N)$, the large- N limit is taken with m/N constant. The spins are represented by fermions f^α , $\alpha = 1 \dots 2N$, which transform under the fundamental of $\text{Sp}(2N)$. The holes are described by spinless bosons b , $c_i^\alpha = f_i^\alpha b_i^\dagger$. The local constraint of the $t - J$ model acquires the form

$$f_{i\alpha}^\dagger f_i^\alpha + b_i^\dagger b_i = m. \quad (2.2)$$

Here we will only discuss states being half-filled at zero doping, $m = N$. The average hole concentration δ is determined by

$$\frac{1}{N_s} \sum_i f_{i\alpha}^\dagger f_i^\alpha = N(1 - \delta) \quad (2.3)$$

where N_s denotes the (infinite) number of lattice sites. Within the $\text{Sp}(2N)$ generalization of the system, the spin operators \mathbf{S}_i become fermion bilinears times the traceless generators of $\text{Sp}(2N)$, the Hamiltonian (2.1) takes the form

$$\begin{aligned} \mathcal{H}_t &= \sum_{i>j} \left[-\frac{t_{ij}}{N} b_i f_{i\alpha}^\dagger f_j^\alpha b_j^\dagger + \text{H.c.} \right] \\ &\quad + \sum_i \lambda_i \left(f_{i\alpha}^\dagger f_i^\alpha + b_i^\dagger b_i - N \right) + \mu \sum_i \left(b_i^\dagger b_i - N\delta \right), \\ \mathcal{H}_J &= \sum_{i>j} \left[-\frac{J_{ij}}{2N} \left(\mathcal{J}^{\alpha\beta} f_{i\alpha}^\dagger f_{j\beta}^\dagger \right) \left(\mathcal{J}_{\gamma\delta} f_j^\delta f_i^\gamma \right) \right] \\ \mathcal{H}_V &= \sum_{i>j} \frac{V_{ij}}{N} b_i^\dagger b_i b_j^\dagger b_j \end{aligned} \quad (2.4)$$

where we have split $\mathcal{H}_{tJ} = \mathcal{H}_t + \mathcal{H}_J$ for convenience. The Lagrange multipliers λ_i enforce the local occupation constraint, and μ fixes the average hole density. $\mathcal{J}^{\alpha\beta}$ denotes the antisymmetric $\text{Sp}(2N)$ tensor:

$$\mathcal{J}^{\alpha\beta} = \mathcal{J}_{\alpha\beta} = \begin{pmatrix} & & & & 1 \\ & & & & -1 \\ & & & 1 & \\ & & -1 & & \\ & & & & \ddots \\ & & & & & \ddots \end{pmatrix} \quad (2.5)$$

We remind the reader that \mathcal{H} given in eq. (2.4) reduces to eq. (2.1) for the “physical” case of $N = 1$.

In the limit $N = \infty$ at zero temperature the bosons b_i condense, $\langle b_i \rangle = \sqrt{N} b_i$, so b_i^2 is the hole density and $N(1 - b_i^2) = \langle n_i \rangle$ the charge density at site i . The exclusion of double occupancies in the $N = 1$ case is now represented by the on-site constraint $\langle n_i \rangle \leq N$ since $b_i^2 > 0$. The long-range nature of Coulomb interaction requires the introduction of a background charge of magnitude

δ on each lattice site for the total system to be charge-neutral. The interaction is decoupled by the introduction of the link fields Q_{ij} with the saddle-point values

$$NQ_{ij} = \langle \mathcal{J}^{\alpha\beta} f_{i\alpha}^\dagger f_{j\beta}^\dagger \rangle = \frac{1}{b_i b_j} \langle \mathcal{J}^{\alpha\beta} c_{i\alpha}^\dagger c_{j\beta}^\dagger \rangle. \quad (2.6)$$

The Q_{ij} represent the complex bond pairing amplitudes. We note that $Q_{ij} = Q_{ji}$, and the phases of the Q_{ij} are only fixed up to a global gauge transformation, $f_i \rightarrow f_i e^{i\Theta}$, which leads to $Q_{ij} \rightarrow Q_{ij} e^{-2i\Theta}$. However, the plaquette operator Π_Q , which can be defined as $\Pi_Q = Q_{12} Q_{23}^* Q_{34} Q_{41}^*$ for the sites 1...4 at the corners of a unit square, is a gauge-invariant object.

At the saddle point the Hamiltonian takes the form

$$\begin{aligned} \mathcal{H}_t &= \sum_{i>j} \left[-t_{ij} b_i b_j f_{i\alpha}^\dagger f_j^\alpha + \text{H.c.} \right] \\ &\quad + \sum_i \lambda_i \left(f_{i\alpha}^\dagger f_i^\alpha + N b_i^2 - N \right) + \mu N \sum_i (b_i^2 - \delta), \\ \mathcal{H}_J &= \sum_{i>j} \left[-\frac{J_{ij}}{2} \left(\mathcal{J}^{\alpha\beta} f_{i\alpha}^\dagger f_{j\beta}^\dagger Q_{ij}^* + \text{H.c.} - N |Q_{ij}|^2 \right) \right] \\ \mathcal{H}_V &= \sum_{i>j} N V_{ij} (b_i^2 - \delta)(b_j^2 - \delta). \end{aligned} \quad (2.7)$$

which is bilinear in the fermions and can be solved by a Bogoliubov transformation. The saddle point solution is found by minimizing the total free energy with respect to b_i and Q_{ij} at fixed average fermion occupation and hole density. The saddle-point equations have been solved numerically with unit cell sizes up to 32 sites. The Coulomb repulsion term in the large- N limit is purely “classical”, i.e., it does not involve the fermions. Using the lattice Fourier transforms $V_{\mathbf{k}}$ and $n_{\mathbf{k}}$ of interaction and charge distribution respectively, the Coulomb contribution to the energy can be re-written as

$$\mathcal{H}_V = N_s N \sum_{\mathbf{k}} V_{\mathbf{k}} n_{\mathbf{k}} n_{-\mathbf{k}} \quad (2.8)$$

The interaction $V_{\mathbf{k}} = V \sum_{\mathbf{R} \neq 0} e^{i\mathbf{k}\mathbf{R}} / |\mathbf{R}|$ behaves as $\sim k^{-1}$ for small $k = |\mathbf{k}|$, but becomes negative around the center of the Brillouin zone. (Note that there is no on-site contribution from V , $V_{ii} = 0$, since the occupation constraint is already taken care of by the local chemical potential λ_i .)

The numerical determination of the minimum energy configuration in the large- N limit consists of two nested loops: (i) Starting from an initial guess for Q_{ij} , b_i , λ_i the fermionic Hamiltonian is diagonalized using a discrete momentum grid (32^2 is sufficient for unit cells up to 8 sites). The expectation values $\langle f_{i\alpha}^\dagger f_{j\beta}^\dagger \rangle$ provide new values for the Q_{ij} , new b_i are obtained from $b_i^2 = 1 - \langle f_{i\alpha}^\dagger f_i^\alpha \rangle / N$, and the average chemical is adjusted (by a simple bisection step) to match the doping level. This is repeated until convergence is reached. (ii)

The optimum charge distribution within the unit cell of N_c sites is found by minimizing the total energy [obtained in loop (i)] w.r.t. the differences in the chemical potentials $\tilde{\lambda}_i = \lambda_i - \lambda_1$. This is a minimum search in a $(N_c - 1)$ -dimensional space and can be performed by standard methods. To account for the possible existence of more than one saddle point the initial link field values Q_{ij} are chosen randomly, and several sets of initial conditions are used to identify the saddle point corresponding to the *global* minimum energy.

A. Ground states at $N = \infty$

The results of our large- N calculation can be summarized as follows: First, at $\delta = 0$ along A_1 we find the fully dimerized, insulating spin-Peierls (or 2×1 bond charge density wave) solution⁵⁹ in which $|Q_{ij}|$ is non-zero only on the bonds shown in Fig. 1.

At non-zero doping δ the “bare” large- N $t - J$ model shows phase separation for a large range of parameters t/J , see Ref. 5. This tendency to phase separation (into a hole-rich region and a fully dimerized half-filled region) at $V = 0$ is an important ingredient of our study. With the inclusion of \mathcal{H}_V the phase separation becomes “frustrated”, as emphasized in Refs. 52–54, and the competition of the energy scales t , J , and V leads to various kinds of charge ordering phenomena. Different ground state phases may be realized depending on the strength on the Coulomb interaction. The details of these solutions will be described in the next subsections.

Fig. 3 shows a representative phase diagram containing a cut along the V - δ plane of the parameter space for fixed $t/J = 1.25$. Phase diagrams for other parameter values are shown in Figs. 6 and 7. The inclusion of additional model parameters as a biquadratic exchange interaction can lead to further ground state phases, these will be described in Sec. II B.

Let us start the discussion of Fig. 3 with large doping. Here no phase separation tendency is present, the ground state charge distribution is homogeneous. The magnetic interaction together with the (infinite) on-site repulsion leads to pairing in the $d_{x^2-y^2}$ channel. Moving to smaller doping, the system encounters a phase separation instability at $V = 0$, i.e., the holes are expelled because the magnetic interaction favors a fully dimerized half-filled configuration. The Coulomb repulsion counteracts (frustrates) this phase separation tendency⁵² leading to microscopic charge ordering below a certain hole concentration, $\delta < \delta_{\text{Stripe}}$. The important point now is that the kinetic energy disfavors crystal-like states where the holes are essentially localized. Instead, the holes form “stripes” where hopping in one dimension is still possible. Furthermore, the tendencies to fermion pairing on one hand and to dimerization on the other hand are still present. Consistent with this picture, our numerical search always yielded lowest energy states with \mathcal{C} and

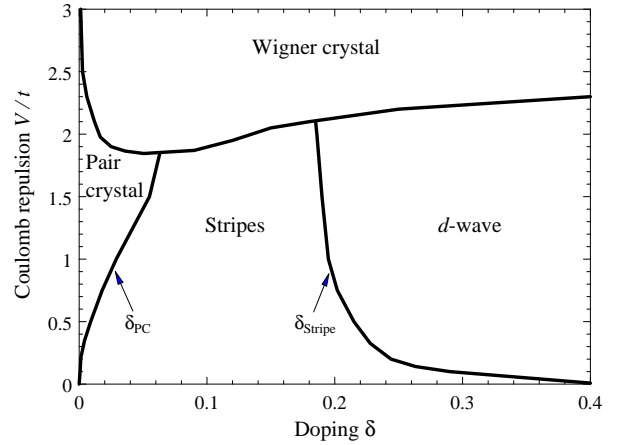


FIG. 3. Ground state phase diagram of \mathcal{H} at $N = \infty$, $t/J = 1.25$. Except for the d -wave superconductor all states have \mathcal{C} broken. The “stripe” states have coexisting charge density wave order and superconductivity; the crystal states are insulating. The thick lines denote phase transitions being first-order in the large- N limit. Within the charge-ordered phases there are numerous additional transitions at which the detailed nature of the \mathcal{C} symmetry breaking changes - these are not shown. The left and right boundaries of the stripe phase define $\delta_{\text{PC}}(V)$ and $\delta_{\text{Stripe}}(V)$, see text.

\mathcal{S} broken, in a region $\delta_{\text{PC}} < \delta < \delta_{\text{Stripe}}$ and for small values of the Coulomb repulsion V . These states consist of *bond-centered charge density waves*^{36,6} (stripes) which co-exist with superconductivity. The effect of the kinetic energy becomes less pronounced when the doping is further decreased. Eventually, for extremely small doping, $\delta < \delta_{\text{PC}}(t, J, V)$, and non-zero repulsion V the lowest energy state is an insulating crystal of Cooper pairs which breaks \mathcal{C} symmetry. Such a state arises from the combination of charge ordering and pairing tendencies. Depending upon the parameter values t , t' , J and V also a doped spin-Peierls state may be realized at small and/or intermediate doping. For strong Coulomb repulsion between the charges (large V region in Fig. 3) one expects that hopping as well as pairing (mediated by the magnetic interaction) will become unimportant. Then the situation resembles a low-density electron gas (where the potential energy dominates over the kinetic energy), and the ground state becomes a Wigner crystal built of single charges.

We continue with a more detailed description of the characteristics of the mean-field ground states.

1. Homogeneous superconductor

At doping levels smaller than a critical $\delta_{\text{PS}}(t, J)$ the “bare” $t - J$ model in the large- N limit shows phase separation⁵ as explained above. [Note $\delta_{\text{PS}}(t, J) = \delta_{\text{Stripe}}(t, J, V = 0)$.] In contrast, for $\delta > \delta_{\text{PS}}$ and small V the ground states have uniform site charge distribu-

tions. These states include a doped spin-Peierls state (2×1 unit cell, see below) at relatively small δ , and states with a single site per unit cell which are homogeneous superconductors. They can be characterized by two link field values Q_x and Q_y . In particular, one finds a d -wave superconductor with $Q_x = -Q_y$ at intermediate δ (~ 20 -50%), and an extended s^* -wave superconductor with $Q_x = Q_y$ for larger δ . The excitation spectrum of the d -wave superconductor has four nodes whereas the s^* -wave phase is fully gapped.

Note that for $t/J < 0.3$ the critical doping level δ_{PS} is in fact zero, so \mathcal{H}_{tJ} does not show phase separation (and no stripes for $V > 0$) at very small t/J . Also, in the regime of small t/J the d -wave superconductor is replaced by a state with $s^* + id_{x^2-y^2}$ symmetry, i.e., the link fields obey $Q_y = Q_x e^{i\theta}$ with a continuously varying phase θ . Here the quasiparticle spectrum is again fully gapped, furthermore time-reversal symmetry \mathcal{T} is broken.

The described results for the homogeneous states are identical to the ones obtained in Ref. 5. Similar states are also found for large values of $|t'/t|$ where the tendency to phase separation is suppressed, see Sec. II B.

2. Spin-Peierls state

The spin-Peierls state which breaks \mathcal{C} is found as ground state of the undoped system in the large- N limit. For $\delta = 0$ its energy per site is given by $E_{SP}/(NN_s) = -J/4$. Only one of the four link fields of the 2×1 unit cell is non-zero, i.e., the square lattice is completely covered by dimers.

The corresponding doped state is the lowest-energy state with a *homogeneous* site-charge distribution in the small doping regime⁵. The link fields in x direction Q_{1x}, Q_{2x} have different magnitudes reflecting the dimerization, whereas $Q_{1y} = Q_{2y}$. The fields cannot be made real simultaneously in any gauge, so the doped state breaks time-reversal invariance \mathcal{T} and is fully gapped. However, if we restrict our attention to states which preserve \mathcal{T} , then there exists a region of small dimerization, $|Q_{1x} - Q_{2x}| \ll |Q_{1x}|$, near the transition to a d -wave state where the spectrum has 4 gapless points. Note that this state which has coexisting superconducting and spin-Peierls order can be considered as a 2×1 bond charge density wave with the hole densities being equal on all sites. Related states have been studied in other approaches^{60,11}, but they find spin-Peierls order in a Fermi liquid, not a superconductor.

3. States with stripe charge order

The saddle-point solutions at small doping, $\delta_{PC} < \delta < \delta_{Stripe}$, and not too large V , break lattice translation symmetry \mathcal{C} and can be described as bond-centered charge

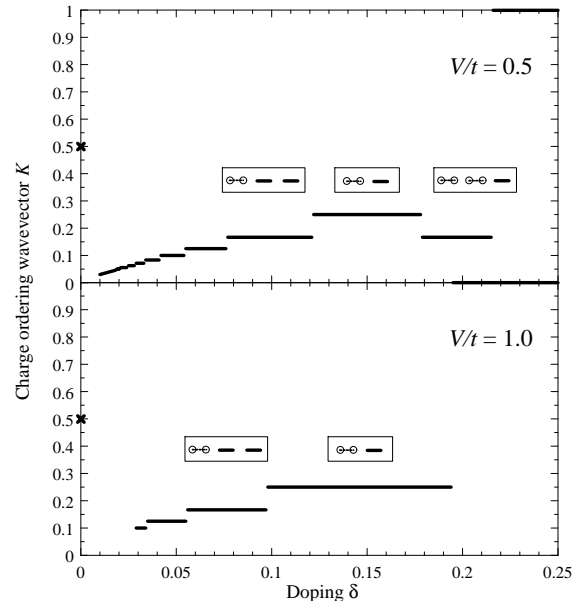


FIG. 4. The charge-ordering wavevector, K , (in reciprocal lattice units) as a function of δ at $N = \infty$ for $t/J = 1.25$ (Fig. 3), and two different strengths of the Coulomb repulsion $V/t = 0.5$ and 1.0 . For the stripe states as illustrated in Fig. 1 we have $K = 1/p$, the spin-Peierls state has $K = 1/2$ at $\delta = 0$. The $K = 1$ value at large δ has \mathcal{C} symmetry restored, and is a pure d -wave superconductor. For very small δ , the ground state is a Wigner crystal of Cooper pairs with incommensurate charge order. The unit cells for the largest plateaus are also shown.

density waves. These states have a $p \times 1$ unit cell, as shown in Fig. 1. We always found p to be an even integer, reflecting the dimerization tendency of the $\delta = 0$ solution.

The holes prefer to segregate in one-dimensional striped structures, i.e., within each $p \times 1$ unit cell, the holes are concentrated on a $q \times 1$ region. The link fields Q in the hole-rich region can be made real and have different signs in x and y direction reminiscent of d -wave pairing correlation in the stripes. Most of the stripe phases are “fully” formed stripes, i.e., the regions between the stripes with a width of $p - q$ have a hole density of zero and are insulating and fully dimerized. In this case the link fields between the stripe sites and the boundary sites of the insulating region vanish. However, for a parameter region close to the transition to a doped spin-Peierls state (see Fig. 6) there occur “partially” formed stripes as ground states. These states have the same kind of charge density modulation as described above, but the hole density in the hole-poor region is not zero, so the system is an anisotropic 2D superconductor even at $N = \infty$. In general, the hole density ρ_ℓ per unit length of each stripe is not of order unity as found in earlier theories but significantly smaller. The values of q and ρ_ℓ are determined primarily by t, J, V ; they depend only weakly on δ . For intermediate values of V where $q = 2$ we found values

of $\rho_\ell \sim 1/2$, here the stripe can be viewed as a ladder with roughly $1/4$ hole per site. In general, smaller values of V yield larger values of q ; the limit $V \rightarrow 0$ leads to $q \rightarrow \infty$ which reflects the tendency to phase separation in the “bare” $t - J$ model.

The main effect of varying the total hole density is a change of p and therefore of the stripe distance. We note that the stripes do not survive in the limit $\delta \rightarrow 0$ ⁶¹: for $\delta < \delta_{\text{PC}}$ the ground state changes to an insulating Wigner crystal of Cooper pairs. However, for small V , δ_{PC} is very small, $\delta_{\text{PC}} \sim \exp(-1/V)$. For $\delta_{\text{PC}} \ll \delta \ll \delta_{\text{Stripe}}$, we find an approximate proportionality $p \sim 1/\delta$, which also implies that ρ_ℓ is nearly independent of δ . The evolution of the ordering wavevector $K = 1/p$ with δ is shown in Figs. 4, 6, 7, there are plateaus for each even integer number p . Our large- N theory only found “stripe” states in which K was quantized at the rational plateaus in Fig. 4. The reason for p, q being even and for the plateaus is easily identified as the strong dimerization tendency of the system. The columnar arrangement of the spin-Peierls singlets immediately leads to the “staircase”-like curve shown in Figs. 4, 6, 7. However, for smaller N we expect that irrational, incommensurate, values of K will appear, and interpolate smoothly between the plateau regions.

For most values of t, J , and V there is a large plateau at $p = 4$ around doping $\delta = 1/8$, and, for some parameter regimes, this is the last state before \mathcal{C} is restored at large δ ; indeed $p = 4$ is the smallest value of p for which our mean-field theory has solutions with b_i not spatially uniform. Experimentally^{62,63}, a pinning of the charge order at a wavevector $K = 1/4$ is observed, and we consider it significant that this value emerges naturally from our theory.

It is worth pointing out that the hole density ρ_ℓ per unit length of stripe is not exactly pinned at one value which means that the stripes are *not* incompressible. The hole density varies continuously within each plateau but jumps discontinuously as the transition is made from one plateau to the next.

There are strong pairing correlations between the holes in each q -width region. Strictly speaking, for $N = \infty$ each q -width stripe above is a one-dimensional superconductor, while the intervening $(q - p)$ -width regions are insulating. However, fluctuation corrections will couple with superconducting regions, yielding an effective theory discussed in Section VII of Ref. 64 with their dimensionless parameter $K \sim N$. This implies that Josephson pair tunneling between the one-dimensional superconductors is a relevant perturbation at sufficiently large N , leading to a two-dimensional anisotropic superconducting ground state, and should allow good metallic conduction above the superconducting transition temperature. These characteristics are consistent with observations⁶⁵ on $\text{La}_{2-x-y}\text{Nd}_y\text{Sr}_x\text{CuO}_4$.

The quasiparticle spectrum in the striped phases is always fully gapped because of the presence of superconductivity. Except for the partially striped phases where

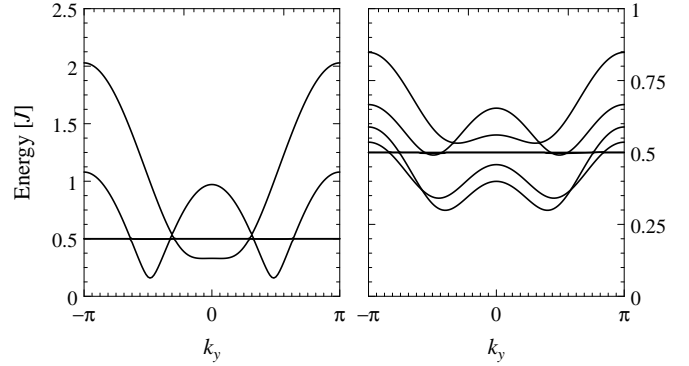


FIG. 5. Fermionic mean-field excitation spectrum in fully striped phases, $t/J = 1.25$. The spectrum is independent of k_x , the momentum perpendicular to the stripes. Left: $q = 2$ phase with $\rho_\ell = 0.8$. Right: $q = 4$ phase with $\rho_\ell = 0.6$. In the second case the bandwidth is much smaller due to the smaller doping level in the stripes (ρ_ℓ/q). The flat bands at energy $J/2$ correspond to excitations of localized dimers in the undoped regions.

the fermion spectrum shows a weak dependence on the momentum k_x perpendicular to the stripes⁶, the spectrum of the stripe phases is k_x -independent. The fermion spectrum in the partially striped phases were displayed in Ref. 6, and in Fig. 5 we show the quasiparticle bands for the fully striped cases. The spectrum consists of two contributions: The excitations of the fully dimerized undoped regions correspond to removing one fermion from a localized dimer, the energy cost is $J/2$ and of course momentum-independent. The stripes of width q give rise to q one-dimensional dispersing bands where the gap is determined by the pairing amplitude of order J , and the total bandwidth is given by $4t\rho_\ell/q$ where ρ_ℓ is the linear hole density per unit stripe as above. The stripe excitations therefore lie in the gap of the spin-Peierls state; their properties are entirely determined by ρ_ℓ and q (and the model parameters t and J). Upon increasing the doping level δ within one of the plateaus in Fig. 4 the superconducting gap decreases slightly since the link fields Q decrease, and the position of the dispersion minimum changes corresponding to the Fermi momentum. The transitions between the plateaus arise from level crossings, i.e., there is no critical dynamics associated with them. At the transition from one plateau to the next, ρ_ℓ decreases discontinuously, leading to an increase in the gap and so on. If the stripe width q changes at a plateau transition then the number of dispersing bands will also change, see Fig. 5.

At this point we briefly discuss earlier mean-field calculations^{20–22} which predicted an inhomogeneous charge distribution in the ground state of the Hubbard and related models. These computations were based on the observation that large- S mean-field theories of doped antiferromagnets (S denotes the size of the spin) show charge density wave instabilities – the same applies to the large- N theory discussed here. An important dif-

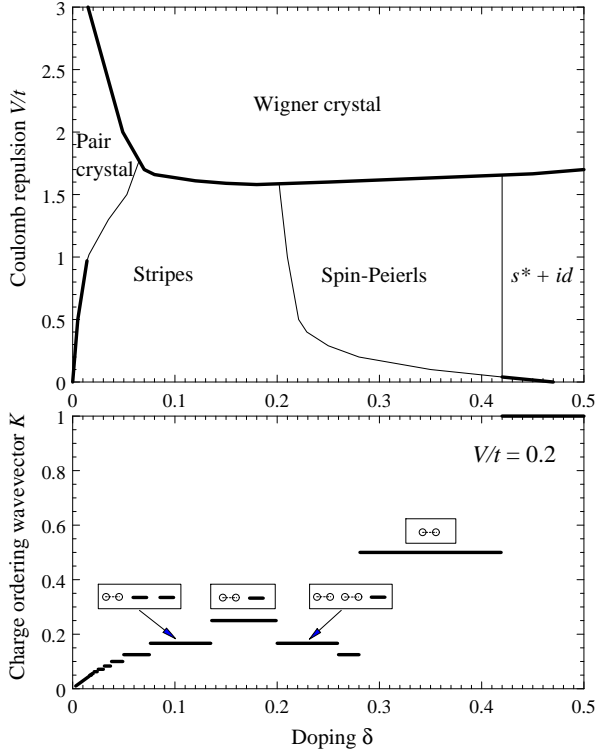


FIG. 6. Same as in Figs. 3 and 4, but for $t/J = 0.5$. Upper panel: Ground state phases of \mathcal{H} as function of doping and Coulomb repulsion. Thick and thin lines denote first-order and second-order transitions, respectively. Lower panel: Charge-ordering wavevector, K , (in reciprocal lattice units) for $V/t = 0.2$. For $28\% < \delta < 42\%$ the ground state is the doped spin-Peierls state breaking \mathcal{C} and \mathcal{S} ; it has a uniform site-charge distribution and a 2×1 unit cell.

ference, however, is the character of the stripes. The early mean-field calculations for the Hubbard model^{20–22} predict insulating, site-centered stripes with a hole density of unity within the hole-rich regions; the experimentally found stripe states in the cuprates are, however, either metallic or superconducting. In contrast to these early mean-field results, the present large- N computations yield superconducting, bond-centered stripes, and it would be useful for future experiments to detect this distinction between bond- and site-centering. Let us discuss this difference more precisely for the case $p = 4$. For the site-centered stripe, the hole density per unit length in each column of sites takes values $\rho_1, \rho_2, \rho_3, \rho_2$ before repeating periodically (where ρ_{1-3} are some three distinct densities); this is the configuration usually assumed in most experimental papers. In contrast, for the bond-centered state, these densities take the values $\rho_1, \rho_1, \rho_2, \rho_2$, and this also appears to be compatible with existing observations. The bond-centering is important in the present computation for enhancing pairing correlations, which are responsible for superconducting/metallic transport in the direction parallel to the stripes.

Possible differences in the spin dynamics between

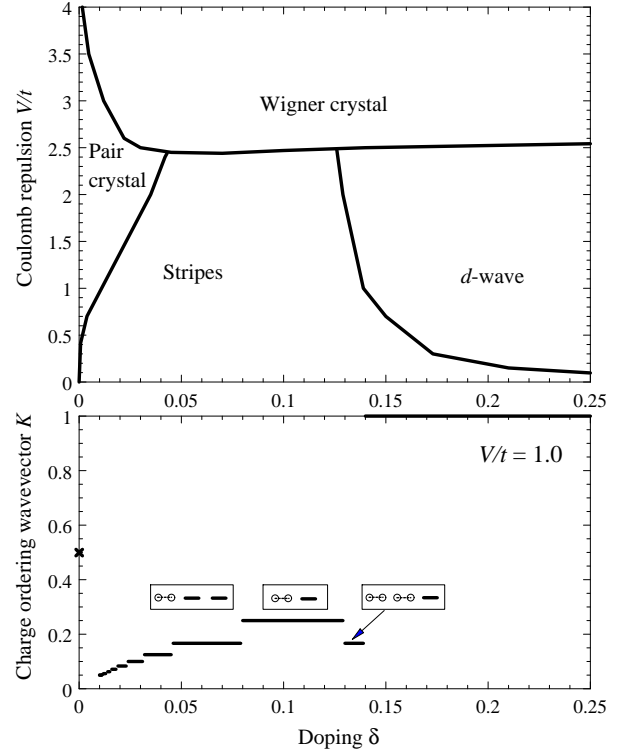


FIG. 7. Same as in Figs. 3 and 4, but for $t/J = 2.5$. Upper panel: Ground state phases of \mathcal{H} as function of doping and Coulomb repulsion. Lower panel: Charge-ordering wavevector, K , (in reciprocal lattice units) for $V/t = 1.0$.

bond- and site-centered striped phases have been discussed by Tworzydło *et al.*². They argued that the magnetic domains between the stripes can be described by spin ladders with either an even or odd number of legs; these two cases lead to very different spin fluctuation spectra.

We note that a very recent NQR experiment⁶⁶ indicates a charge distribution which has some features consistent with the bond-centered state: they find only two inequivalent sites associated with the stripes, and a density in the hole-rich region which is considerably smaller than 0.5.

4. Wigner crystals of Cooper pairs

For very small doping the “stripe” states become unstable with respect to further \mathcal{C} breaking. This leads to two-dimensional insulating states with \mathcal{S} restored, which can be characterized as Wigner crystals of Cooper pairs⁵². In the large- N limit, the Cooper pair crystals consist of pairs of adjacent sites with non-zero hole density and a non-zero bond amplitude Q between them; the remaining sites of the square lattice form singlet bonds as in the fully dimerized, undoped spin-Peierls state. The occurrence of such pair crystal states is intimately related to the dimerization tendency of the system: In a

pair crystal the repulsion energy is much smaller than a stripe state, and the hole-rich sites still form dimers leading to a non-zero contribution from \mathcal{H}_{tJ} . (At $N = \infty$ the hole density on the sites of each pair is not exactly unity, $b_i^2 < 1$, this is an artifact of the large- N limit. For physical values of N the physical system will certainly have two electrons per pair.)

To minimize the repulsion energy, the hole pairs want to form a triangular Wigner lattice (with a lattice constant $\sim \sqrt{\delta}$). However, in the present problem the hole positions have to be on the underlying square lattice. This leads to incommensurate structures where the pairs form an approximate triangular lattice. The energy per site in this state at small δ is given by $E_{\text{PC}}/(NN_s) = -J/4 - \alpha\delta$ where α contains contributions from t , J , and V .

We note here that there are also crystal-like insulating saddle-point solutions with clusters of sites with non-zero hole density. These “charge islands” can be considered as an integer number of Cooper pairs bound together – the described pair crystals are the smallest possible islands. Larger islands occur at small doping, they replace the pair crystal phases shown in the phase diagrams at small hopping t . We have not systematically examined all possible “island” phases because large islands require large unit cells in the numerical calculation. However, by estimating the ground state energy of the “island” phases we have checked that stripe phases are always favored in the experimentally interesting doping regime, $8\% < \delta < 20\%$.

Summarizing these findings, the frustration of complete phase separation by V leads to two possible scenarios of charge clusters with “smaller” size: (i) stripes which are 1d objects, i.e., the charges are confined in one direction (note that finite T may melt the stripe order leaving behind finite length parts of stripes; strong impurity influence may also break up stripes into segments), and (ii) islands which can be considered as bound states of Cooper pairs – here the charges are confined in both directions. The calculations show that for physical values of t/J and not too small doping δ the stripe scenario (i) is favored due to the larger kinetic energy of the holes in the stripes.

5. Wigner crystals of single charges

For large V the Coulomb repulsion dominates over t and J which leads to the appearance of Wigner crystal states – here the crystal consists of *single charges*. The holes minimize the Coulomb energy by forming a crystal-like structure – this is similar to the charge ordering in a low-density electron gas. The lowest Coulomb energy is again reached for the case where the charges form a triangular lattice with a Wigner lattice constant $\sim \sqrt{\delta}$, however, the hole positions have to coincide with the sites of the underlying square lattice. Therefore, the states

at large Coulomb repulsion V will have structures incommensurate with the square lattice, i.e., a (infinitely) large unit cell with holes sitting on a fraction $1/\delta$ of the sites ($b_i^2 = 1$). These sites form an approximate triangular Wigner lattice, all other sites are half-filled ($b_i^2 = 0$) and form dimerized bonds. (The calculation shows that at finite values of V/J the competition of exchange and Coulomb energies at $N = \infty$ leads to hole densities on the sites of the Wigner lattice being smaller than unity, $b_i^2 < 1$, and to a distortion of the ideal dimer pattern in the link fields Q near each hole site. This again is an artifact of the condensation of the slave bosons in the large- N limit.)

The kinetic energy in the Wigner crystal state vanishes. The exchange energy per site is given by $-J/4 \times (1-\delta)$ at low δ since $(1-\delta)$ is the number of sites remaining for singlet formation. It is important to note that the Coulomb energy is negative, i.e., $\langle \mathcal{H}_V \rangle \sim -\gamma\delta^{1/2} < 0$ with $\gamma \sim V$. So we can estimate the energy per site for small δ to be $E_{\text{WC}}/(NN_s) = -J/4(1-\delta) - \gamma\delta^{3/2}$.

B. Influence of additional model parameters

The calculations presented so far show that the tendency to stripe formation at low doping is a very robust feature of the $t - J - V$ model at $N = \infty$. In the following we discuss the influence of the inclusion of further processes into the Hamiltonian.

1. Longer-range hopping

We start with an additional next-nearest neighbor hopping t' which is supposed to be important in certain cuprate superconductors. The large- N calculations show that the results are nearly independent of t' as long as it is small, $|t'/t| < 0.3$. Larger values of t' of either sign suppress the tendency to phase separation in the “bare” model (without \mathcal{H}_V). This in turn means that the stripe instability is weakened; the stripe region in the phase diagram shrinks, it is shifted to lower doping and lower values of V . This is consistent with e.g. the findings of White and Scalapino³⁶.

2. Biquadratic exchange

We have also considered the addition of a biquadratic spin exchange

$$H_4 = \frac{\kappa J}{4N^3} \sum_{\langle i,j \rangle} (\mathbf{S}_i \cdot \mathbf{S}_j)^2 \quad (2.9)$$

to the Hamiltonian (2.4) for general N . The strength of the biquadratic interaction is given by κJ . For the physical case $N = 1$ the biquadratic exchange term simply

reduces to $\mathbf{S}_i \cdot \mathbf{S}_j + \text{const}$, but for larger N it contains exchange processes involving eight fermions¹⁶. For the total coupling of two (isolated) spins to be antiferromagnetic there is an upper limit for κ which is given by $\kappa < 2$ for any N ¹⁶. In the large- N limit the decoupling can be done in two steps, it turns out that no new link fields are necessary. At the saddle point the additional term takes the form:

$$H_4 = \frac{\kappa J}{8} \sum_{\langle i,j \rangle} |Q_{ij}|^2 \left(2\mathcal{J}^{\alpha\beta} f_{i\alpha}^\dagger f_{j\beta}^\dagger Q_{ij}^* + \text{H.c.} - 3N|Q_{ij}|^2 \right) \quad (2.10)$$

As discussed in Ref. 16 such a biquadratic exchange term weakens the tendency to dimerization. In fact, in the $\text{SU}(N)$ saddle-point approach it can be used to stabilize a staggered flux phase; it is expected to find a similar effect on the hole-poor regions of the stripe states⁶⁷.

In the undoped system, we find that the $N = \infty$ ground state changes from spin-Peierls (at $\kappa = 0$) to a box phase for $0 < \kappa < 1.13$, and then to a “flux”-like phase for $\kappa > 1.45$. (Some intermediate phase occurs for $1.13 < \kappa < 1.45$.) All phases at $J > 0$ can be described within a 2×2 unit cell. The box phase has non-zero link fields Q around isolated plaquettes of four sites each, all other link fields vanish¹⁶. In the “flux”-like phase all Q are equal in magnitude, their phases can be made real by a gauge transformation, and the expectation value of the plaquette operator Π_Q is real and negative. However, unlike in the $\text{SU}(N)$ case there is no direction associated with the Q link fields. A direct interpretation in terms of a flux is therefore not possible. The described mean-field solutions are identical with the results of Marston and Affleck for the $\text{SU}(N)$ Heisenberg model¹⁶. In fact, by applying a generalized particle-hole transformation it can be shown that the mean-field equations for the undoped system are equivalent for both $\text{SU}(2N)$ and $\text{Sp}(2N)$ cases.

Turning to finite doping, we find that all homogeneous phases are unstable w.r.t. phase separation at $V = 0$ and low doping. The inclusion of V leads to stripe states similar to the ones described in Sec. II A 3 for all values of κ . The hole concentration ρ_ℓ in the stripes is again determined by the microscopic parameters, and is found to be between 0.2 and 0.5 for reasonable values of t , J , and V . The stripes are one-dimensional superconductors, for most of the parameter values the bond amplitudes Q within the stripes can be made real and reflect d -wave pairing correlations [at larger V and intermediate δ there is a small region with $(s^* + id)$ -like pairing in the stripes]. The Q fields in the insulating regions between the stripes reflect the structure of the undoped ground state: At small non-zero κ one finds a box-like structure whereas $\kappa > 1.45$ gives rise to a more homogeneous distribution of the Q which can be understood as flux-like arrangement with distortions at the boundaries (stripes). Interestingly, in the latter case there can occur non-zero link fields Q between the stripes and the undoped region

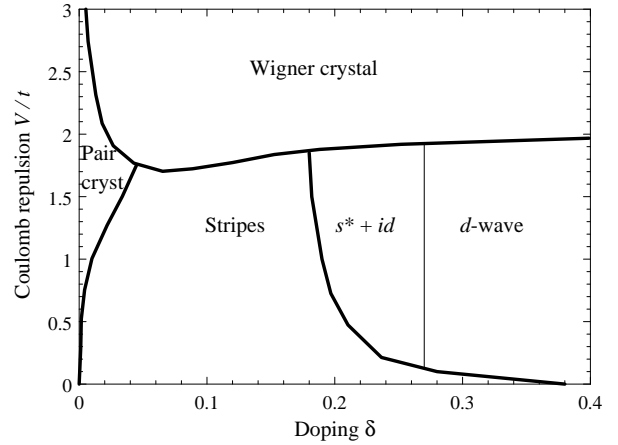


FIG. 8. Ground state phase diagram for the $\text{Sp}(2N)$ $t-J$ model with biquadratic exchange term as function of doping and Coulomb repulsion, $t/J = 0.75$, $\kappa = 1.5$.

(leading to longer-ranged spin correlations), but these disappear for larger hole concentration in the stripes.

At larger doping the stripes are disfavored, the ground state becomes a homogeneous superconductor with either d -wave or $s^* + id$ symmetry. Compared to the case $\kappa = 0$, the tendency to phase separation is slightly weakened by the introduction of the biquadratic exchange, the region of stripe ground states shrinks. A sample phase diagram is shown in Fig. 8. Note that the transition from d -wave to $s^* + id$ symmetry with decreasing doping is accompanied with the opening of a gap in the fermionic spectrum (and with spontaneous \mathcal{T} breaking).

3. Next-nearest neighbor exchange

To explore further possible symmetries of the superconducting order parameter (which is represented by the link fields Q in the mean-field theory) we consider an additional next-nearest neighbor exchange $J' > 0$. Note that the inclusion of such a frustrating next-nearest neighbor exchange between pairs of sites on the same sublattice is straightforward within the present $\text{Sp}(2N)$ mean-field theory since the same representation of $\text{Sp}(2N)$ is employed for spins on both sublattices [in contrast to the bosonic $\text{SU}(N)$ approach]. The new interaction is decoupled similar to the nearest-neighbor interaction as described at the beginning of Sec. II; this leads to diagonal link fields Q'_{ij} . The model with hopping terms t and t' , exchange processes J and J' as well as biquadratic exchange strengths κJ and $\kappa J'$ shows a number of new ground state phases at the mean-field level, among them superconductors with mixed order parameters, spin-Peierls and flux-like phases as well as charge-ordered states.

As an example, we show the phase diagram for $t/J = 1.0$, $J'/J = 0.4$, and $\kappa = 1.5$ in Fig. 9. The un-

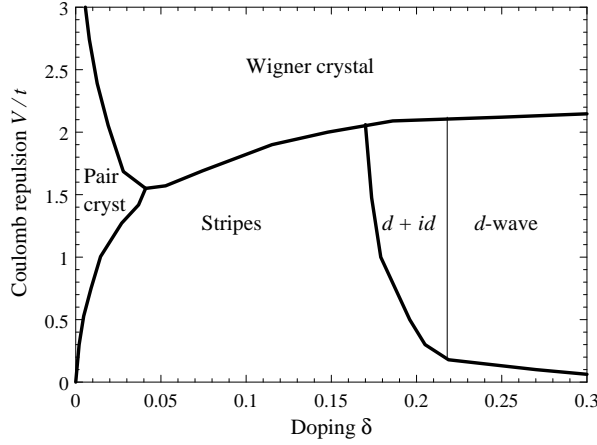


FIG. 9. Ground state phase diagram for the $\text{Sp}(2N)$ $t - J - J' - V$ model with biquadratic exchange term as function of doping and Coulomb repulsion; $t/J = 1.0$, $J'/J = 0.4$, $t' = 0$, $\kappa = 1.5$. $d+id$ denotes the \mathcal{T} -breaking superconductor with $(d_{x^2-y^2} + id_{xy})$ -wave symmetry.

doped system has a large ground state degeneracy, small doping produces stripe states due to the phase separation instability in the absence of Coulomb repulsion V . The stripes disappear at larger doping, leading to a superconductor with a homogeneous charge distribution. First we find a $(d_{x^2-y^2} + id_{xy})$ -wave superconductor; further increasing δ leads to a pure $d_{x^2-y^2}$ state. The $(d_{x^2-y^2} + id_{xy})$ -wave state has a fully gapped spectrum and breaks time reversal symmetry. It is characterized by four Q link fields which obey $Q_x = -Q_y$, $Q'_{11} = -Q'_{1,-1}$ and $Q'_{11} = i\epsilon Q_x$. Here, ϵ is a real value measuring the mixing of both d -wave order parameters. At the transition line between the $(d_{x^2-y^2} + id_{xy})$ state and the pure $d_{x^2-y^2}$ -wave state the ϵ vanishes continuously.

4. Alternative interaction decoupling

There has been recent interest^{68,69} in possible ground states which spontaneously break time-reversal symmetry \mathcal{T} and show circulating currents¹⁴⁻¹⁸ (doped “flux” phases). Such states can be characterized as orbital magnets; if the current direction around each unit cell alternates in sign between adjacent cells one obtains an orbital antiferromagnet. To explore possible realizations of such states within our saddle-point approach we extend the Hamiltonian by an interaction term which provides decoupling in the particle-hole channel in the large- N limit. It has the form $(-\bar{J}_{ij})/(2N) (f_{i\alpha}^\dagger f_{j\alpha})(f_{j\beta}^\dagger f_{i\beta})$ which also reduces to $\mathbf{S}_i \cdot \mathbf{S}_j + \text{const}$ for $N = 1$. The interaction is decoupled by link fields χ which take the values

$$N\chi_{ij} = N\chi_{ji}^* = \langle f_{i\alpha}^\dagger f_{j\alpha} \rangle \quad (2.11)$$

at the saddle point. In contrast to the Q fields these new fields χ_{ij} specify a direction for the link (ij) . For the

undoped case the phases of the χ are gauge-dependent, but the plaquette operator $\Pi_\chi = \chi_{12}\chi_{23}\chi_{34}\chi_{41}$ is again a gauge-invariant object. In the doped system, the fields χ are directly connected with the current transported through one link, $j_{ij} = 2N \text{Im}\chi_{ij}$, so their phases are meaningful.

At the saddle point the Hamiltonian containing the interaction \bar{J} takes the form

$$\bar{\mathcal{H}}_J = \sum_{i>j} \left[-\frac{\bar{J}_{ij}}{2} (f_{i\alpha}^\dagger f_{j\alpha} \chi_{ij}^* + \text{H.c.} - N|\chi_{ij}|^2) \right] \quad (2.12)$$

which is formally a contribution to the fermion hopping. We also include a corresponding biquadratic interaction which can be decoupled in the particle-hole channel leading to

$$\bar{H}_4 = \frac{\kappa \bar{J}}{8} \sum_{\langle i,j \rangle} |\chi_{ij}|^2 \left(2f_{i\alpha}^\dagger f_{j\alpha} \chi_{ij}^* + \text{H.c.} - 3N|\chi_{ij}|^2 \right) \quad (2.13)$$

The mean-field equations show that a magnetic interaction of the type (2.12) is equivalent to the decoupling done within a $\text{SU}(2N)$ large- N approach to the antiferromagnet. The sum of both terms, $\bar{\mathcal{H}}_J + \bar{H}_4$, contains both possible factorizations (particle-particle and particle-hole) of the four-fermion interaction term. It is therefore equivalent to an unrestricted Hartree-Fock treatment of the original Heisenberg Hamiltonian for $N = 1$ written in terms of auxiliary fermions, provided that $J_{ij} = \bar{J}_{ij}$. In the following, we will discuss the large- N limit and treat J and \bar{J} as independent parameters, concentrating on the region where $J \sim \bar{J}$. Varying the ratio $x \equiv \bar{J}/(\bar{J} + J)$ can be viewed as continuous interpolation between the $\text{Sp}(2N)$ ($x = 0$) and $\text{SU}(2N)$ ($x = 1$) approaches to the antiferromagnet.

For $x = 1/2$ ($J = \bar{J}$) and doping $\delta = 0$, we find a large ground state degeneracy which has also been reported earlier in unrestricted Hartree-Fock treatment of the Heisenberg antiferromagnet⁷⁰. The degeneracy can be lifted by the introduction of a biquadratic exchange $\kappa > 0$ which leads to box-like phases having a 2×2 unit cell. These states have non-zero values of both the Q and χ link fields.

Turning to finite doping, we find no phase separation instability at $x = 1/2$ independent of κ — at zero or small V states with a homogeneous site charge distribution always have lower energy than inhomogeneous states; there are no stripe states at $x = 1/2$. The ground state at low doping is either a spin-Peierls state (at $\kappa = 0$) or box-like ($\kappa > 0$), for larger doping it becomes a pure d -wave superconductor. The phase diagram for $\kappa = 0$ is shown in Fig. 10. The spin-Peierls state shows dimerization in both the Q and the χ fields with a pattern as described in Sec. II A 2. It is interesting to note that the doped spin-Peierls state does not break time reversal symmetry \mathcal{T} , so the Q fields can be made real by a gauge transformation (in contrast to the spin-Peierls state occurring

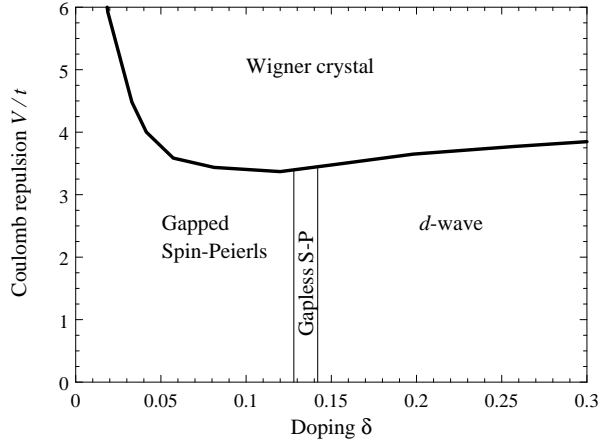


FIG. 10. Ground state phase diagram for the $t - J$ model with interactions \mathcal{H}_J and $\bar{\mathcal{H}}_J$, $t/J = 1$, $x = 1/2$ ($\bar{J} = J$), $\kappa = 0$ (no biquadratic exchange). There are *two* spin-Peierls phases shown: At larger doping the dimerization is small leading to gapless spectrum with four nodes. Upon decreasing δ the dimerization increases, and when it exceeds some critical value, the spectrum becomes gapped: the gap opens when the nodal points collide in pairs at points on the lines $k_y = \pm\pi/2$ in the extended Brillouin zone.

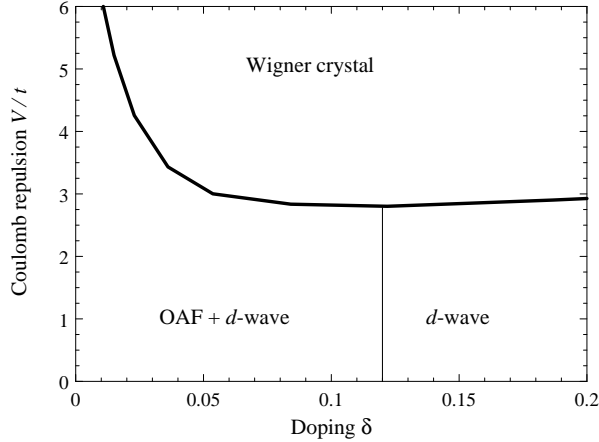


FIG. 11. Ground state phase diagram for the $t - J$ model with interactions \mathcal{H}_J and $\bar{\mathcal{H}}_J$ which are both supplemented by a biquadratic exchange, $\kappa = 1.5$. The remaining parameters are $t/J = 1.25$, $x = 0.6$ ($\bar{J} = 1.5J$). OAF denotes the \mathcal{T} -breaking orbital antiferromagnet with staggered circulating currents around each plaquette. At $\delta = 0$ we have the staggered flux state.

in the “pure” $\text{Sp}(2N)$ case which is always \mathcal{T} breaking). Similarly, the doped box state for $x = 1/2$ also preserves \mathcal{T} .

As one further example, we describe the ground states at $x = 0.6$. The undoped system without biquadratic exchange ($\kappa = 0$) again shows a large degeneracy. Values of $0 < \kappa < 1.4$ lead to a box-like phase. For $\kappa > 1.4$ we find the staggered flux phase as ground state, here all χ are equal in magnitude and the plaquette operators Π_χ

have the negative real expectation values. The particle-particle link fields Q vanish for any κ .

At finite doping, there is again no phase separation tendency at $x = 0.6$. For $\kappa = 0$ the ground state phases are spin-Peierls at small δ and d -wave at larger δ , whereas small non-zero κ produces box-like ground states. Interesting phases occur for $\kappa > 1.4$ as shown in the phase diagram in Fig. 11: The staggered flux phase evolves to an orbital antiferromagnet with a two-site unit cell and circulating currents (given by $\text{Im } \chi$) in each plaquette with alternating direction between adjacent plaquettes. This state is unstable to pairing¹⁷: the Q fields acquire non-zero, real values leading to a \mathcal{T} -breaking state with coexisting orbital antiferromagnetism and d -wave superconductivity⁶⁹. We note that this coexistence occurs here at the mean-field level, this can be contrasted to other mean-field theories⁷¹ where the flux and d -wave instabilities occur in different orders in a $1/N$ expansion.

For larger doping, the currents vanish, and the ground state becomes a pure d -wave superconductor. All the described states have a gapless excitation spectrum – note here that the flux phase can be interpreted as a $d_{x^2-y^2}$ density wave, implying nodes of the order parameter in the diagonal directions in momentum space.

At very large values of V the dominating repulsion gives rise to Wigner crystal states as described above. However, there are no pair crystal phases for the cases $x = 0.5$ and 0.6 which is related to the absence of phase separation tendencies at these parameter values.

Finally we note that the case $x = 1$, i.e., the “pure” $\text{SU}(N)$ interaction decoupling, leads to phase separation in the absence of Coulomb repulsion V ⁶⁰, and the inclusion of V is expected to produce “striped” ground states⁷².

C. Phase transitions at $N = \infty$

We briefly discuss the nature of the transitions between the various ground state phases at the mean-field level ($N = \infty$).

The transition from a d -wave superconductor, with \mathcal{C} unbroken, to the fully-formed $p \times 1$ stripes discussed above, can either be first-order, or via intermediate states with partial stripe order. In the latter case, there is first a continuous transition to a doped spin-Peierls state with \mathcal{C} symmetry breaking at $p = 2$. To our knowledge a $p = 2$ charge-ordered superconducting state has not been experimentally detected, but a search for one should be worthwhile. Then there is a second second-order transition to $p = 4$ state with partial stripe order, before the fully-formed $p = 4$, $q = 2$ state with intervening insulating stripes appears. In any case, the excitation spectrum in the stripe states is fully gapped. The transitions between the different stripe phases where p changes its value are in general first-order since they arise from level crossings.

At very small hole densities the Cooper pair crystal states are favored over striped states, then the ground state nature changes from one-dimensional to two-dimensional \mathcal{C} breaking. Again, this transition is either first-order or second-order depending on the values of t , J , and V , in the latter case it can be visualized as additional \mathcal{C} breaking in the longitudinal stripe direction.

Finally, the transition to a Wigner crystal phase of single charges at large V is always a first-order transition because the inherent tendency to fermion pairing is broken in the Wigner crystal.

By adding a biquadratic exchange term to the Hamiltonian we found a \mathcal{T} -breaking superconductor with s^*+id symmetry and a gapped spectrum. As displayed in the phase diagram of Fig. 8, it shows a second-order transition to a pure d -wave state with increasing doping. Similarly, the introduction of a second-nearest neighbor exchange J' can lead to a \mathcal{T} -breaking $(d_{x^2-y^2} + id_{xy})$ -wave superconductor which also has a second-order transition to a pure d -wave state with increasing δ , see Fig. 9.

The $SU(2N)$ -like interaction term $\tilde{\mathcal{H}}_J$ (Sec. II B 4) which has to be decoupled in the particle-hole channel leads to other possible transition scenarios. As shown in Fig. 10, a \mathcal{T} -conserving spin-Peierls phase is possible. Then two transitions are found upon decreasing doping: First there is a second-order transition from the d -wave state to a (weakly dimerized) spin-Peierls state where the dimerization sets in. The four nodes of the d -wave phase are preserved, but shift gradually in momentum space. At smaller δ and a “critical” dimerization there is another second-order transition where the spectrum becomes gapped. Turning to the $x = 0.6$ phase diagram of Fig. 11, we note that the transition between the OAF+ d -wave coexistence phase and the pure d -wave state is second-order. Both order parameters have $d_{x^2-y^2}$ symmetry leading to gapless spectra. The \mathcal{T} symmetry is broken in the low doping phase with orbital currents.

III. CONTINUOUS QUANTUM PHASE TRANSITIONS

In Section II C we noted a number of continuous quantum phase transitions in the mean-field phase diagrams of Fig. 3-11. As we discussed in Section I A, for the purposes of understanding the photoemission experiments of Ref 40, we are particularly interested in transitions in class A. Of these, the simplest involve \mathcal{T} symmetry breaking alone, and we will consider these in the first subsection below. Transitions involving breaking of \mathcal{C} symmetry alone are considered next in Section III B. This is followed by a discussion of the onset of staggered flux order in a d -wave superconductor (this transition breaks \mathcal{T} and \mathcal{C} symmetries) in Section III C.

A. d -wave to $(s^* + id)$ -wave or $(d_{x^2-y^2} + id_{xy})$ -wave

A continuous transition between a d -wave superconductor and a $(s^* + id)$ -wave superconductor appears in the mean-field phase diagram in Fig. 8, and fluctuations in its vicinity will be described below. A very closely related theory applies to the transition between a d -wave superconductor and a $(d_{x^2-y^2} + id_{xy})$ -wave superconductor shown in Fig 9. Indeed, to the order we are computing things, the results for the scaling functions of the two transitions are identical.

We note that a transition between d and $(d_{x^2-y^2} + id_{xy})$ pairing was also considered recently by D.-H. Lee⁷³ using a rather different framework. Lee concluded that the transition was in the universality class of the Ising model in a transverse field; this is equivalent to assuming that the critical theory is described by S_ϕ in (3.3) below, and places the transition in class B. In fact, as we show below, it is also necessary to include fermionic excitations: the complete theory is in (3.7) below, and the transition is in a new universality class which belongs in class A. In a separate recent work, Balatsky *et al.*⁴¹ considered a “clapping” collective mode in a $(d_{x^2-y^2} + id_{xy})$ superconductor: this is an ‘angular’ fluctuation mode expected in a state with well-formed d_{xy} pairing induced by an external magnetic field; in contrast we are interested here in *spontaneous* fluctuations to $(d_{x^2-y^2} + id_{xy})$ order, which will be dominated by ‘amplitude’ fluctuations represented by our field ϕ below.

We begin by establishing notation, and reviewing the familiar physics of the low-energy fermionic quasiparticles in a d -wave superconductor. For the most part, we will follow the notation of Balents *et al.*⁴³. The low energy excitations appear at four points in the Brillouin zone: (K, K) , $(-K, K)$, $(-K, -K)$, and $(K, -K)$. We denote the components of the electron annihilation operator, c_a , in their vicinity by f_{1a} , f_{2a} , f_{3a} , f_{4a} respectively, where $a = \uparrow, \downarrow$ is the electron spin component. Now introduce the 4-component Nambu spinors $\Psi_1 = (f_{1a}, \varepsilon_{ab} f_{3b}^\dagger)$ and $\Psi_2 = (f_{2a}, \varepsilon_{ab} f_{4b}^\dagger)$ where ε_{ab} is an antisymmetric tensor with $\varepsilon_{\uparrow\downarrow} = 1$. The action for the fermionic excitations in the d -wave superconductor is then

$$S_\Psi = \int \frac{d^d k}{(2\pi)^d} T \sum_{\omega_n} \Psi_1^\dagger (-i\omega_n + v_F k_x \tau^z + v_\Delta k_y \tau^x) \Psi_1 + \int \frac{d^d k}{(2\pi)^d} T \sum_{\omega_n} \Psi_2^\dagger (-i\omega_n + v_F k_y \tau^z + v_\Delta k_x \tau^x) \Psi_2. \quad (3.1)$$

Here τ^α are Pauli matrices which act in the fermionic particle-hole space, $k_{x,y}$ measure the wavevector from the nodal points and have been rotated by 45 degrees from the axes of the square lattice, and v_F , v_Δ are velocities.

Let us now consider the transition to the $(s^* + id)$ -wave superconductor. This involves only a Z_2 symmetry breaking of the \mathcal{T} symmetry, and so the order parameter is a real scalar field, ϕ . In the presence of a non-zero,

spacetime-independent ϕ , the superconducting gap function takes the form

$$\langle c_{k\uparrow} c_{-k\downarrow} \rangle = \Delta_0 (\cos k_x - \cos k_y) + i\phi (\cos k_x + \cos k_y). \quad (3.2)$$

The superconducting order parameter also has a single overall complex phase, but because the superfluid stiffness is finite, its fluctuations can be neglected in the critical theory. On general symmetry grounds, we can write down the following effective action for ϕ fluctuations

$$S_\phi = \int d^d x d\tau \left[\frac{1}{2} (\partial_\tau \phi)^2 + \frac{c^2}{2} (\nabla \phi)^2 + \frac{s_0}{2} \phi^2 + \frac{u_0}{24} \phi^4 \right]; \quad (3.3)$$

Here c is a velocity, s_0 is the parameter which tunes the system across the transition, and u_0 measures the quartic self-interaction of the order parameter. Normally, in the absence of strict particle-hole symmetry, a term with a first-order time derivative can potentially appear in S_ϕ ; however, ϕ is a real field, and the only possible relevant term, $\phi \partial_\tau \phi = (1/2) \partial_\tau \phi^2$, is a total derivative and integrates to zero.

The final piece of the action is the coupling between ϕ and the fermionic excitations. This can be easily deduced from (3.2), and the standard pairing interaction between $\Delta(k)$ and the electrons. In the vicinity of the nodal points, this coupling reduces to the very simple expression³⁵ (we are assuming here that $K \neq \pi/2$, as is the case experimentally⁴⁰, so that $(\cos k_x + \cos k_y)$ does not vanish at the nodal points)

$$S_{\Psi\phi} = \int d^d x d\tau \left[\lambda_0 \phi \left(\Psi_1^\dagger \tau^y \Psi_1 + \Psi_2^\dagger \tau^y \Psi_2 \right) \right]. \quad (3.4)$$

The remainder of this subsection will consider the properties of the theory $S_\Psi + S_\phi + S_{\Psi\phi}$. Before we embark on this case, we note the generalization to the case of a transition to $d_{x^2-y^2} + id_{xy}$ order: in this case (3.2) is replaced by

$$\langle c_{k\uparrow} c_{-k\downarrow} \rangle = \Delta_0 (\cos k_x - \cos k_y) + i\phi \sin k_x \sin k_y; \quad (3.5)$$

in the vicinity of the nodal points, instead of (3.4), we obtain³⁵

$$\tilde{S}_{\Psi\phi} = \int d^d x d\tau \left[\lambda_0 \phi \left(\Psi_1^\dagger \tau^y \Psi_1 - \Psi_2^\dagger \tau^y \Psi_2 \right) \right]. \quad (3.6)$$

The only change is the relative minus sign between the two terms, which arises from the changing sign of the factor $\sin k_x \sin k_y$ in (3.5) between the nodal points; it is this change which is responsible for the non-zero spin Hall conductance of the $d_{x^2-y^2} + id_{xy}$ state³⁵. The properties of the theory $S_\Psi + S_\phi + \tilde{S}_{\Psi\phi}$ are very closely related to that of $S_\Psi + S_\phi + S_{\Psi\phi}$; indeed, at the one-loop order we compute things here, there is no difference between the

theories, and our results can be applied equally to the transition to either $s^* + id$ or $d_{x^2-y^2} + id_{xy}$ order.

Our renormalization group analysis is closely related to that discussed by Zinn-Justin⁷⁴. We will mainly restrict our study to the case in which all the velocities in $S_{\Psi,\phi}$ are equal to each other. By a suitable choice of the scale of time we can then set $c = v_F = v_\Delta = 1$ at the outset. Deviations from exactly equal velocities will be considered in Section III A 1 below, and in future work. With exactly equal velocities, the action is actually Lorentz invariant and so we must have the dynamic exponent $z = 1$; this will value of z will be implicitly assumed in the remainder of this paper. We introduce notation to make the Lorentz invariance explicit. We map $\Psi_2 \rightarrow (\tau^x + \tau^z) \Psi_2 / \sqrt{2}$, and define $\bar{\Psi}_{1,2} = -i\tau^y \Psi_{1,2}^\dagger$, and introduce Lorentz index $\mu = \tau, x, y$. Then $S_\Psi + S_\phi + S_{\Psi\phi}$ can be written in the compact Lorentz-invariant form

$$S_{s^*+id} = \int d^D x \left(i\bar{\Psi}_1 \partial_\mu \gamma^\mu \Psi_1 + i\bar{\Psi}_2 \partial_\mu \gamma^\mu \Psi_2 + \frac{1}{2} (\partial_\mu \phi)^2 + \frac{s_0}{2} \phi^2 + \frac{u_0}{24} \phi^4 - i\lambda_0 \phi (\bar{\Psi}_1 \Psi_1 - \bar{\Psi}_2 \Psi_2) \right), \quad (3.7)$$

where $D = d + 1$, and $\gamma^\mu = (-\tau^y, \tau^x, \tau^z)$. We note that there is also a corresponding action $S_{d_{x^2-y^2}+id_{xy}}$ which (using (3.6)) differs only in having a relative plus sign between the couplings of $\bar{\Psi}_1 \Psi_1$ and $\bar{\Psi}_2 \Psi_2$ to ϕ .

We now proceed with the renormalization group analysis of S_{s^*+id} or $S_{d_{x^2-y^2}+id_{xy}}$. We will present the results using the field-theoretic method as it leads to a more streamlined discussion of finite temperature properties. To this end, we introduce the wavefunction renormalizations

$$\begin{aligned} \phi &= Z_b^{1/2} \phi_R \\ \Psi_{1,2} &= Z_f^{1/2} \Psi_{1,2R} \end{aligned} \quad (3.8)$$

and the coupling constant renormalizations

$$\begin{aligned} \lambda_0 &= \frac{\mu^{\epsilon/2}}{S_D^{1/2}} \frac{Z_\lambda}{Z_f Z_b^{1/2}} \lambda \\ u_0 &= \frac{\mu^\epsilon}{S_D} \frac{Z_u}{Z_b^2} u \end{aligned} \quad (3.9)$$

where μ is a renormalization momentum scale and $S_D = 2/(\Gamma(D/2)(4\pi)^{D/2})$.

One loop calculations of the renormalization constants using minimal subtraction of poles in $\epsilon = 4 - D = 3 - d$ yield

$$\begin{aligned} Z_b &= 1 - \frac{4\lambda^2}{\epsilon} \\ Z_f &= 1 - \frac{\lambda^2}{2\epsilon} \\ Z_\lambda &= 1 + \frac{\lambda^2}{\epsilon} \\ Z_u &= 1 + \frac{3u}{2\epsilon} - \frac{48\lambda^4}{u\epsilon}. \end{aligned} \quad (3.10)$$

From these we obtain the beta-functions (note that we are using the field-theorists' definition of the beta function⁷⁴, and these are opposite in sign to those normally used by condensed matter physicists):

$$\begin{aligned}\beta(\lambda) &= -\frac{\epsilon}{2}\lambda + \frac{7}{2}\lambda^3 \\ \beta(u) &= -\epsilon u + \frac{3}{2}u^2 + 8u\lambda^2 - 48\lambda^4.\end{aligned}\quad (3.11)$$

These equations have the infrared stable fixed point

$$\begin{aligned}\lambda^{*2} &= \frac{\epsilon}{7} \\ u^* &= \frac{16\epsilon}{21}\end{aligned}\quad (3.12)$$

which controls the physics in the vicinity of the quantum critical point. In particular, the fields acquire the anomalous dimensions

$$\begin{aligned}\eta_b &= 4\lambda^{*2} \\ \eta_f &= \lambda^{*2}/2\end{aligned}\quad (3.13)$$

which will play an important role in the spectral functions to be discussed below.

In the first subsection below, we will consider the consequences of unequal velocities. The next subsection will describe the $T > 0$ quantum critical spectral response functions of the fixed point (3.13).

1. Unequal velocities

The full treatment of the problem with unequal velocities is considerably more complicated than the simple renormalization group analysis above, and is deferred to future work. It is entirely possible that there are other non-Lorentz-invariant fixed points describing the critical theory: however, apart from differences in the details of the scaling functions, the qualitative properties of such fixed points should be quite similar to the Lorentz-invariant case explored in more detail in Section III A 2.

We will restrict our attention here to perturbations which break Lorentz invariance in a linear stability analysis of the Lorentz-invariant fixed point. Such an analysis was also carried out in Ref. 43, but the authors do not appear to have performed the proper decomposition of the perturbations into the appropriate eigenoperators, as is required to obtain the correct scaling dimensions.

It is important to classify the perturbations in terms of irreducible representations of the Lorentz symmetry of the fixed point. For the velocity differences, these are the symmetric, traceless, second-rank Lorentz tensors. So we consider the following perturbation to the action $S_\Psi + S_\phi + S_{\Psi\phi}$:

$$S_a = \int d^D x \left[\tilde{g}_{\mu\nu} \left(\partial_\mu \phi \partial_\nu \phi - \frac{\delta_{\mu\nu}}{D} (\partial_\rho \phi)^2 \right) \right]$$

$$\begin{aligned}& + i g_{\mu\nu}^{(1)} \bar{\Psi}_1 \left(\frac{\partial_\mu \gamma^\nu + \partial_\nu \gamma^\mu}{2} - \frac{\delta_{\mu\nu}}{D} \partial_\rho \gamma^\rho \right) \Psi_1 \\ & + i g_{\mu\nu}^{(2)} \bar{\Psi}_2 \left(\frac{\partial_\mu \gamma^\nu + \partial_\nu \gamma^\mu}{2} - \frac{\delta_{\mu\nu}}{D} \partial_\rho \gamma^\rho \right) \Psi_2 \Big].\end{aligned}\quad (3.14)$$

It is crucial that the tensors above are traceless: this ensures, at linear order, that such perturbations do not mix with terms already in the Lorentz-invariant action, and with redundant operators which can be removed by a rescaling of the fields which are being integrated over.

It is a simple matter to compute the one-loop renormalization group flow equations to the terms in (3.14). We find

$$\begin{pmatrix} \beta(\tilde{g}_{\mu\nu}) \\ \beta(g_{\mu\nu}^{(1)}) \\ \beta(g_{\mu\nu}^{(2)}) \end{pmatrix} = \lambda^2 \begin{pmatrix} 4 & -2 & -2 \\ -1/3 & 1/3 & 0 \\ -1/3 & 0 & 1/3 \end{pmatrix} \begin{pmatrix} \tilde{g}_{\mu\nu} \\ g_{\mu\nu}^{(1)} \\ g_{\mu\nu}^{(2)} \end{pmatrix}. \quad (3.15)$$

Clearly, we need the eigenvalues and eigenvectors of the matrix of coefficients in (3.15). First, note that there is an eigenvector, $(1, 1, 1)$, with zero eigenvalue. This is expected, and its presence is an important check on our calculation—it corresponds to the perturbation of simply changing *all* velocities by the same amount: such a redundant perturbation can be absorbed by a rescaling of spacetime co-ordinates, and does not modify any of the physics.

The other eigenvalues and eigenvectors correspond to physical differences in the velocities. The eigenvector $(0, 1, -1)$ has eigenvalue $1/3$ and corresponds to the perturbation in which v_F and v_Δ are made unequal. So such a perturbation is irrelevant in the infrared, with scaling dimension $-\lambda^{*2}/3 = -\epsilon/21$. The final eigenvector, $(-12, 1, 1)$, induces a difference between the velocities of the fermions and bosons, and this perturbation is more strongly irrelevant: the scaling dimension is $-13\lambda^{*2}/3 = -13\epsilon/21$.

So we have established that the Lorentz-invariant fixed point is at least linearly stable to velocity differences. However, the scaling dimension of the leading irrelevant operator is quite small $(-\epsilon/21)$, and this could lead to very slowly decaying transients in the critical behavior.

2. $T > 0$ spectral functions

The problem of computing $T > 0$, quantum critical, spectral functions in 2+1 dimensions is one of considerable complexity. Even though the non-linear couplings at the fixed point, (3.3), are small for small ϵ , the low frequency response at $T > 0$ cannot be computed in a bare ϵ expansion. This is because the limits $\epsilon \rightarrow 0$ and $\omega \rightarrow 0$ do not commute, and there are spurious low-frequency singularities in the bare ϵ expansion: this is discussed further in Appendix A. For the case of a scalar field alone, this problem of $T > 0$ dynamics was addressed in Refs. 75,13 by a two-step procedure involving a mapping to a quasi-classical problem. Here we shall use the

insight gained from these previous, controlled studies to motivate a simple self-consistent one-loop theory for computing the low frequency relaxation rates. In contrast to the previous studies⁷⁵, we are aided here by the fact that damping appears already at the one-loop level in S_{s^*+id} or $S_{d_{x^2-y^2}+id_{xy}}$, and this simplifies the solution of the self-consistent equations.

We shall be interested in the following retarded response functions in the “quantum critical”¹³ regime:

$$\begin{aligned} G_f(k, i\omega_n) &= Z_f^{-1} \langle \Psi_1(k, \omega_n) \Psi_1^\dagger(k, \omega_n) \rangle \\ G_b(k, i\omega_n) &= Z_b^{-1} \langle \phi(k, \omega_n) \phi(-k, -\omega_n) \rangle. \end{aligned} \quad (3.16)$$

After analytic continuation to real frequencies G_f satisfies the scaling form in (1.1), and an analogous result for G_b with $f \rightarrow b$.

For $\omega \gg T$ or $k \gg T$, the response functions in (3.16) equal their $T = 0$ results, and these can be computed in the bare ϵ expansion. A familiar computation in the one loop renormalized theory gives us

$$\begin{aligned} G_f(k, \omega) &= C_f \mu^{-\eta_f} \frac{\omega + k_x \tau^z + k_y \tau^x}{[k^2 - (\omega + i0)^2]^{1-\eta_f/2}} \\ G_b(k, \omega) &= C_b \mu^{-\eta_b} \frac{1}{[k^2 - (\omega + i0)^2]^{1-\eta_b/2}} \end{aligned} \quad (3.17)$$

where $C_{f,b}$ are constants given by

$$\begin{aligned} C_f &= 1 - \lambda^{*2}/4 + \dots \\ C_b &= 1 - 2\lambda^{*2} + \dots \end{aligned} \quad (3.18)$$

Clearly, (3.17) obeys the scaling form (1.1).

Next we consider the more difficult case where ω, k are of order T or smaller. Here we shall proceed by using an ansatz for the low frequency form of the Green’s functions: this ansatz is motivated by the results of the corresponding low frequency regime in a number of other models^{75,13}, especially the exactly solvable Ising chain in a transverse field¹³. In these studies, it was found that, provided the number of order parameter components was not large, the low frequency spectral functions had a simple relaxational form, that of degrees of freedom in a simple dissipative medium. In the present situation, we have a single scalar order parameter, and can expect that a similar situation should apply. We therefore make the ansatz

$$\begin{aligned} G_f(k, \omega) &= \left(\frac{\mu}{T}\right)^{-\eta_f} \frac{\omega + i\Gamma_f + k_x \tau^z + k_y \tau^x}{k^2 - (\omega + i\Gamma_f)^2} \\ G_b(k, \omega) &= \left(\frac{\mu}{T}\right)^{-\eta_b} \frac{1}{k^2 - (\omega + i\Gamma_b)^2}. \end{aligned} \quad (3.19)$$

where $\Gamma_{f,b}$ are damping frequencies we need to determine. The functional form for G_b in (3.19) was found to be a remarkably good fit to the low frequency portion of the known exact result for the spectral function of an Ising chain in a transverse field^{13,76}. A further rationale

behind (3.19) is that we have only included terms in the self energy of the fields which are lower powers of the frequency than those already present in the free propagator, and which are consistency with the requirement that all spectral functions are smooth at $\omega = 0$ for $T > 0$. It is precisely these low frequency powers which acquire a singular form in the bare ϵ expansion, and so we are forced to use the self-consistent approach to be described below. Comparing (3.19) with (1.1) we see that consistency demands that $\Gamma_{f,b}$ be universal numbers times temperature. The purpose of the remainder of this subsection is to determine the universal numbers Γ_f/T and Γ_b/T . Before turning to this, let us also quote, the form of (3.19) in imaginary frequencies

$$\begin{aligned} G_f(k, i\omega_n) &= \left(\frac{\mu}{T}\right)^{-\eta_f} \frac{i\omega_n + i\Gamma_f \text{sgn}(\omega_n) + k_x \tau^z + k_y \tau^x}{k^2 + (|\omega_n| + \Gamma_f)^2} \\ G_b(k, i\omega_n) &= \left(\frac{\mu}{T}\right)^{-\eta_b} \frac{1}{k^2 + (|\omega_n| + \Gamma_b)^2} \end{aligned} \quad (3.20)$$

The damping represented by $\Gamma_{f,b}$ arises from interactions between the thermally excited bosons and fermions. The typical excitation will have energy of order T , and as the damping is dominated by the lowest energy excitations, the typical interaction vertex will have external frequencies at order T or lower. Motivated by this, we develop a perturbation theory for the interactions not in terms of the bare vertices, but in terms of the full interaction vertices between the excitations. At the one-loop level, the damping terms arise from the λ_0 interactions alone: however rather than expanding in powers of λ_0 , we will express the self energy in powers of the full three-point irreducible vertex, Λ_3 between one boson (ϕ) and two Fermi ($\Psi_{1,2}^\dagger, \Psi_{1,2}$) fields. A convenient choice is to use the zero momentum vertex between a Bose field at zero frequency, and Fermi fields at the minimum Matsubara frequency of $\epsilon_n = \pi T$. Bare perturbation theory for this vertex gives

$$\Lambda_3 = \lambda_0 - \lambda_0^3 \int \frac{d^d k}{(2\pi)^d} T \sum_{\omega_n} \frac{1}{(k^2 + \omega_n^2)(k^2 + (\epsilon_n + \omega_n)^2)} \quad (3.21)$$

where ω_n is a fermionic frequency. General scaling arguments from renormalization theory^{75,77} show that at the fixed point the exact result for the vertex obeys

$$\Lambda_3 = \frac{T^{\epsilon/2}}{Z_f Z_b^{1/2}} \left(\frac{\mu}{T}\right)^{\eta_f + \eta_b/2} C_3 \quad (3.22)$$

where C_3 is a *universal* number. Evaluating the frequency sums and the momentum integrals in (3.21), and expressing everything in terms of renormalized couplings at the fixed point, and collecting low order terms in ϵ , we find that (3.22) is indeed obeyed, with the universal number

$$C_3 = \frac{1}{S_{d+1}^{1/2}} (\lambda^* + 0.374367\lambda^{*3} + \dots) \quad (3.23)$$

To proceed with the damping calculation, we write down the structure of the self-consistent one-loop equations in terms of the Green's functions of the bare fields; from (3.16) these are $G_f^B = Z_f G_f$ and $G_b^B = Z_b G_b$. We define the self energies by

$$\begin{aligned} (G_f^B)^{-1} &= -i\omega_n + k_x \tau^z + k_y \tau^x - \Sigma_f^B \\ (G_b^B)^{-1} &= \omega_n^2 + k^2 + s_0 - \Sigma_b^B. \end{aligned} \quad (3.24)$$

The self-consistent, one-loop expression for the self energies, expressed in terms of Λ_3 , are

$$\begin{aligned} \Sigma_f^B(k, \omega_n) &= \Lambda_3^2 \int \frac{d^d p}{(2\pi)^d} T \sum_{\epsilon_n} \tau^y G_f^B(p, \epsilon_n) \tau^y \\ &\quad \times G_b^B(k - p, \omega_n - \epsilon_n) \\ \Sigma_b^B(k, \omega_n) &= -2\Lambda_3^2 \text{Tr} \int \frac{d^d p}{(2\pi)^d} T \sum_{\epsilon_n} \tau^y G_f^B(p, \epsilon_n) \tau^y \\ &\quad \times G_f^B(k + p, \omega_n + \epsilon_n) \end{aligned} \quad (3.25)$$

We will now express this in terms of renormalized quantities. First we note by comparing (3.24) with (3.19, 3.20) that we only need the imaginary part of the self energies at small real frequencies; in particular, the damping co-efficients can be expressed as

$$\begin{aligned} \Gamma_f &= \left(\frac{\mu}{T}\right)^{-\eta_f} Z_f \lim_{\omega \rightarrow 0} \text{Im} \Sigma_f^B(0, \omega) \\ \Gamma_b &= \left(\frac{\mu}{T}\right)^{-\eta_b} Z_b \lim_{\omega \rightarrow 0} \frac{\text{Im} \Sigma_b^B(0, \omega)}{2\omega} \end{aligned} \quad (3.26)$$

We now insert (3.20), (3.22), (3.25) into (3.26). To our satisfaction, we find that all factors of the renormalization factors $Z_{b,f}$ and the scale μ precisely cancel out, and the remaining expressions involve only universal quantities. Performing the frequency summation in (3.25) and inserting in (3.26) we obtain

$$\begin{aligned} \Gamma_f &= C_3^2 \int_0^\infty \frac{d\Omega}{\pi} \int \frac{d^d k}{(2\pi)^d} \frac{T^\epsilon}{\sinh(\Omega/T)} \\ &\quad \times \text{Im} \left(\frac{1}{k^2 - (\Omega + i\Gamma_b)^2} \right) \\ &\quad \times \text{Im} \left(\frac{\Omega + i\Gamma_f}{k^2 - (\Omega + i\Gamma_f)^2} \right) \\ \Gamma_b &= 2C_3^2 \int_0^\infty \frac{d\Omega}{\pi} \int \frac{d^d k}{(2\pi)^d} \frac{T^{\epsilon-1}}{\cosh^2(\Omega/2T)} \\ &\quad \times \left[\left\{ \text{Im} \left(\frac{\Omega + i\Gamma_f}{k^2 - (\Omega + i\Gamma_f)^2} \right) \right\}^2 \right. \\ &\quad \left. - k^2 \left\{ \text{Im} \left(\frac{1}{k^2 - (\Omega + i\Gamma_f)^2} \right) \right\}^2 \right] \end{aligned} \quad (3.27)$$

A simple dimensional analysis of (3.27) shows that T can be completely scaled out of both equations for all d . The strength of the damping is determined by the dimensionless ratios Γ_f/T and Γ_b/T , and these are completely determined by the dimensionless universal C_3 .

We solved (3.27) numerically in $d = 2$. The results are $\Gamma_f/T = 0.581$ and $\Gamma_b/T = 0.170$.

B. \mathcal{C} symmetry breaking in a d -wave superconductor

A number of transitions involving \mathcal{C} symmetry breaking in a d -wave superconductor were noted in Section II. These involve the onset of either stripe or spin-Peierls order, and such transitions appear in Figures 3, 7, and 10. In all cases, the order parameter can be identified with scalars Φ_x, Φ_y representing the amplitude of charge density waves with wavevectors $(Q, 0)$ and $(0, Q)$. If Q is commensurate with the underlying lattice, then $\Phi_{x,y}$ are real; otherwise $\Phi_{x,y}$ are complex, with their phases representing the freedom of the charge density wave to slide with respect to the underlying lattice. On general symmetry grounds, we can write down an effective action for $\Phi_{x,y}$, similar to (3.3):

$$\begin{aligned} S_\Phi &= \int d^d x d\tau \left[|\partial_\tau \Phi_x|^2 + |\partial_\tau \Phi_y|^2 + |\nabla \Phi_x|^2 + |\nabla \Phi_y|^2 \right. \\ &\quad + s_0 (|\Phi_x|^2 + |\Phi_y|^2) + \frac{u_0}{2} (|\Phi_x|^4 + |\Phi_y|^4) \\ &\quad \left. + v_0 |\Phi_x|^2 |\Phi_y|^2 \right], \end{aligned} \quad (3.28)$$

where, for now, $\Phi_{x,y}$ can be either real or complex. First-order time derivative terms, like $\Phi_x^* \partial_\tau \Phi_x$, are forbidden here by spatial inversion symmetry under which $\Phi_x \rightarrow \Phi_x^*$, and such a term changes sign after integration by parts.

To complete the theory, we have to consider the coupling of $\Phi_{x,y}$ to the gapless Fermi excitations at wavevectors $(\pm K, \pm K)$. Conservation of momentum implies that there is in fact no long-wavelength coupling between $\Phi_{x,y}$ and $\Psi_{1,2}$ (which is linear in $\Phi_{x,y}$) unless $Q = 2K$. The mean-field studies of Section II always obtained $Q \neq 2K$, and this expected to be the generic behavior. However, we cannot rule out the possibility that there is a mode-locking phenomenon which preferentially condenses a charge density wave at wavevector $Q = 2K$ over a finite range of parameters.

For $Q \neq 2K$, S_Φ is the complete critical theory of the transition: the fermions are not part of the critical theory and so the transition is in class B. The simplest allowed couplings between the fermions and the critical degrees of freedom are terms like $w_0 \int d^d x d\tau |\Phi_x|^2 \Psi_1^\dagger \tau^z \Psi_1$. Simple power counting shows that w_0 has scaling dimension $1/\nu - d$, where ν is the correlation length exponent of the transition described by (3.28). We expect that this ν is greater than that of the $d+1 = 3$ dimensional XY model, which is $\approx 2/3$, and hence w_0 is irrelevant in $d = 2$. By

counting scaling dimensions (or by an explicit perturbative computation) we can deduce that the self energy of the nodal fermions obeys $\text{Im}\Sigma_f^B \sim w_0^2 T^{2d+1-2/\nu}$, and so the damping rate vanishes with a super-linear power of T as $T \rightarrow 0$, as expected for a class B transition.

In the remainder of this section, we consider the class A transition with $Q = 2K$, and both incommensurate (experimentally, and in our mean-field theory, K is incommensurate), so that $\Phi_{x,y}$ are complex. Now a coupling between $\Phi_{x,y}$ and $\Psi_{1,2}$ is possible. Writing down all possible terms consistent with symmetries we obtain⁶

$$S_{\Psi\Phi} = \int d^d x d\tau \left[(\lambda_0 + \zeta_0) \left(\Phi_x \Psi_2^\dagger \tau^z \Psi_1 + \Phi_y \varepsilon_{ab} \Psi_{2a} \tau^x \Psi_{1b} \right) - (\lambda_0 - \zeta_0) \left(\Phi_x \Psi_2^\dagger \tau^x \Psi_1 + \Phi_y \varepsilon_{ab} \Psi_{2a} \tau^z \Psi_{1b} \right) + \text{H.c.} \right] \quad (3.29)$$

The renormalization group analysis of $S_\Psi + S_\Phi + S_{\Psi\Phi}$ parallels that carried out in Section III A, and so we will be brief. The theory can be shown to be Lorentz invariant for $c = v_F = v_\Delta$ and $\zeta_0 = 0$, and so also has $z = 1$. For this Lorentz-invariant case, the renormalization constants, replacing those in (3.10) are

$$\begin{aligned} Z_b &= 1 - \frac{2\lambda^2}{\epsilon} \\ Z_f &= 1 - \frac{\lambda^2}{\epsilon} \\ Z_\lambda &= 1 - \frac{\lambda^2}{\epsilon} \\ Z_u &= 1 + \frac{5u^2 + v^2 - 2\lambda^4}{u\epsilon} \\ Z_v &= 1 + \frac{2v^2 + 4uv - 4\lambda^4}{v\epsilon} \end{aligned} \quad (3.30)$$

(the coupling v has been defined from v_0 following the relationship between u and u_0 in (3.9)), the beta functions, replacing those in (3.11) are

$$\begin{aligned} \beta(\lambda) &= -\frac{\epsilon}{2}\lambda + \lambda^3 \\ \beta(u) &= -\epsilon u + 5u^2 + v^2 + 4u\lambda^2 - 2\lambda^4 \\ \beta(v) &= -\epsilon v + 2v^2 + 4uv + 4v\lambda^2 - 4\lambda^4, \end{aligned} \quad (3.31)$$

and the anomalous dimensions modifying those in (3.13) are

$$\begin{aligned} \eta_b &= 2\lambda^{*2} \\ \eta_f &= \lambda^{*2}. \end{aligned} \quad (3.32)$$

The computation of the $T > 0$ spectral functions proceeds as before, but with the following changes: (i) In (3.21) and (3.23), the λ^3 terms have the opposite sign; (ii) In (3.25), the integrand in the expression for Σ_f^B has a prefactor $2\Lambda_3^2$, while that for Σ_b^B has a prefactor $-\Lambda_3^2$;

(iii) In (3.27), the integrand in the expression for Γ_f has a prefactor $2C_3^2$, while that for Γ_b has a prefactor C_3^2 . The numerical values of the damping coefficients are now $\Gamma_f/T = 1.35$ and $\Gamma_b/T = 0.395$.

C. OAF order in a d -wave superconductor

We discuss here the transition between a d -wave superconductor and the phase with coexisting OAF (or staggered flux) and d -wave superconducting order^{17,69}: such a transition appears in Fig. 11 at $\delta \approx 0.12$. We will show that this transition is in class B (in the notation of Section I A).

As has been emphasized by Nayak⁶⁹, the OAF is characterized by a d -wave order parameter in the particle-hole channel:

$$\langle c_{k+G,a}^\dagger c_{k,a} \rangle = i\phi(\cos k_x - \cos k_y) \quad (3.33)$$

where $G = (\pi, \pi)$ and ϕ is a real order parameter. As in the above subsections, the key issue is the coupling of this order parameter to the fermionic quasiparticles of the d -wave superconductor. As the order parameter carries momentum G , no coupling, linear in ϕ is possible unless the nodal points are at $(\pm K, \pm K)$ with $K = \pi/2$.

For $K \neq \pi/2$ the simplest allowed coupling is $w_0 \int d^d x d\tau \phi^2 \Psi_1^\dagger \tau^z \Psi_1 + \dots$. As we saw in Section III B, such a coupling is irrelevant and places the transition in class B. The damping rate obeys $\text{Im}\Sigma_f^B \sim w_0^2 T^{2d+1-2/\nu_I} \approx T^{1.83}$, where $\nu_I \approx 0.63$ is the correlation length exponent of the Ising model in $d+1=3$ (described by the field theory S_ϕ in (3.3)).

For completeness, let us also consider the special case where $K = \pi/2$. Then, from (3.33) we can compute⁶⁹ the following coupling between ϕ and $\Psi_{1,2}$:

$$\phi \varepsilon_{ab} \left[i\Psi_{1a} \tau^x \partial_y \Psi_{1b} + i\Psi_{2a} \tau^x \partial_x \Psi_{2b} + \text{H.c.} \right]. \quad (3.34)$$

Note that this coupling has one more derivative than those in (3.6) and (3.29); this is a consequence of the vanishing of the factor $(\cos k_x - \cos k_y)$ in (3.33) at the nodal points. Therefore, (3.34) is irrelevant by simple power-counting. A coupling such as (3.34) will not lead to a fermion spectral function obeying (1.1); instead the imaginary part of the fermionic self-energy vanishes as $\text{Im}\Sigma_f^B \sim T^{2+\eta_I}$, where $\eta_I > 0$ is anomalous dimension of the order parameter (ϕ) of the Ising model in $D=3$ spacetime dimensions. So even for $K = \pi/2$, this transition remains in class B.

IV. DISCUSSION

This paper has presented a comprehensive mean-field study of realistic models of the cuprate superconductors.

A representative sample of our results appears in Figs 3-11, and the properties of the phases therein were summarized in Section I. These mean-field results unify many other earlier studies^{14,78,32,16,70,52,5,60,36,71,11} and expose the relationships between them.

A second focus of the paper has been on the second-order quantum phase transitions in Figs 3-11. We paid particular attention to the $T > 0$ fermionic quasiparticle spectra in the vicinity of the nodal points in the Brillouin zone, with the purpose of understanding the observed quantum-criticality in recent photoemission experiments⁴⁰. We divided the transitions into two classes, A and B (described in Section I A), with only those in class A leading to universal damping with ω/T scaling near the nodal points. Particularly appealing examples of class A transitions, for which class A behavior was generic and did not require any special parameter values, were those involving time-reversal (\mathcal{T}) symmetry breaking in a d -wave superconductor: the most important of these are the transitions from d -wave to $(s^* + id)$ -wave or $(d_{x^2-y^2} + id_{xy})$ -wave superconductivity, which appeared in our mean-field phase diagrams. The transition to $(d_{x^2-y^2} + id_{xy})$ order had the additional satisfying feature of very naturally leading to the absence of quantum-critical damping of quasiparticles at momenta (π, k) , (k, π) (with $0 \leq k \leq \pi$), as is found in experiments⁴⁵⁻⁴⁷ below the superconducting critical temperature. However, the transition involving onset of “staggered-flux” (or orbital antiferromagnet) order in a d -wave superconductor, which broke both \mathcal{T} and \mathcal{C} symmetries, was *not* of class A. We note that fermion damping in a model involving \mathcal{T} symmetry breaking has also been examined recently by Varma⁷⁹, although he refers to quantum criticality associated with a transition in a Fermi liquid and not a superconductor. We also examined the onset of “charge stripe-order” (\mathcal{C} symmetry breaking) in the d -wave superconductor: such transitions belonged to class A if the charge ordering wavevector was precisely equal to the separation between two nodal points of the d -wave superconductor. This is a fine-tuning condition, which is also not supported by experiments, and makes the \mathcal{C} breaking transition a less attractive scenario for explaining fermion damping.

So the most viable candidate for the state X in Fig 2 is the $(d_{x^2-y^2} + id_{xy})$ -wave superconductor. For this case, the damping mechanisms appear to divide the fermion excitations into two distinct components. The fermions along the $(1, 0)$, $(0, 1)$ axes are strongly paired in the $d_{x^2-y^2}$ -wave state but are decoupled from the critical order parameter fluctuations (d_{xy}) to the state X : consequently there is negligible damping of these fermions below T_c . On the other hand, the fermions along the $(1, \pm 1)$ axes couple strongly to the d_{xy} order parameter and undergo quantum critical damping as described by (1.1). The situation changes dramatically once we go above T_c . Now phase fluctuations and the proliferation of $hc/2e$ vortices⁸⁰ will strongly scatter the fermions which couple efficiently to the predominant $d_{x^2-y^2}$ or-

der parameter: these are the fermions along $(1, 0)$, $(0, 1)$ directions, while the vortices are largely invisible to the fermions along the $(1, \pm 1)$ directions. Moreover, the antiferromagnetic spin fluctuations, which were responsible for fermion pairing along the $(1, 0)$, $(0, 1)$ axes below T_c , will scatter these same fermions (on the “hot spots”) above T_c ; again, these fluctuations are invisible to the $(1, \pm 1)$ direction fermions because the antiferromagnetic wavevector does not connect the nodal points. Indeed, as we indicated in Section I A, the predominant damping of the $(1, \pm 1)$ direction fermions above T_c continues to arise from the quantum critical d_{xy} fluctuations to the state X : this mechanism applies as long as the quantum-critical scattering length of these fermions remains shorter than the superconducting phase coherence length.

With an eye towards comparisons with photoemission experiments^{40,48,49}, we review our results for the nodal fermionic spectral functions of the class A transitions. As in Ref. 40 we will follow the evolution of the spectral function along a line from the zone center going through the nodal points *e.g.* from $(0, 0)$ along the $(1, 1)$ direction through the nodal point at (K, K) . At the wavevector, $(K + k, K + k)$, our results for (1.1) are contained in the diagonal components of (3.17, 3.19); we express these results in the form

$$G_f(k, \omega) = \left(\frac{\mu}{T}\right)^{-\eta_f} \frac{1}{k - \omega - \tilde{\Sigma}_f}. \quad (4.1)$$

Note that $\tilde{\Sigma}_f$ is strictly not a self-energy (and thus the tilde), as some of the self-energy corrections have already been absorbed into the prefactor of an anomalous power of T in (4.1). We have also set the velocity in the $(1, 1)$ direction to unity.

For small ω, k , our result for $\tilde{\Sigma}_f$ in (3.19) is

$$\tilde{\Sigma}_f = i\Gamma_f \quad ; \quad |\omega| \text{ and } |k| < T, \quad (4.2)$$

where Γ_f/T is a universal number. For the d -wave to $(s^* + id)$ -wave or $(d_{x^2-y^2} + id_{xy})$ -wave transition we estimated $\Gamma_f/T = 0.58$ in Section III A 2, while for the onset of a certain type of \mathcal{C} ordering in a d -wave superconductor we obtained $\Gamma_f/T = 1.35$ in Section III B. We plot the results (4.1, 4.2) in Fig. 12.

For large ω or k , our result is in (3.17). For small η_f , this can be written as

$$\tilde{\Sigma}_f = \frac{\eta_f}{2} \left[(k - \omega) \left(\ln \left(\frac{|\omega^2 - k^2|}{T^2} \right) - 1 \right) + i\pi|\omega - k|\theta(|\omega| - |k|) \right] ; \quad |\omega| \text{ or } |k| \gg T, \quad (4.3)$$

where θ is the unit step function. Note that the imaginary part of $\tilde{\Sigma}_f$ vanishes for $|\omega| \leq |k|$, and, in the present form, this will lead to an infinite spectral density at the threshold $|\omega| = |k|$. However, this is repaired by considering corrections to (4.3). Within the scaling limit of the universal theories being considered here, we evaluate the expression (3.25) in Appendix A; at $T > 0$, but

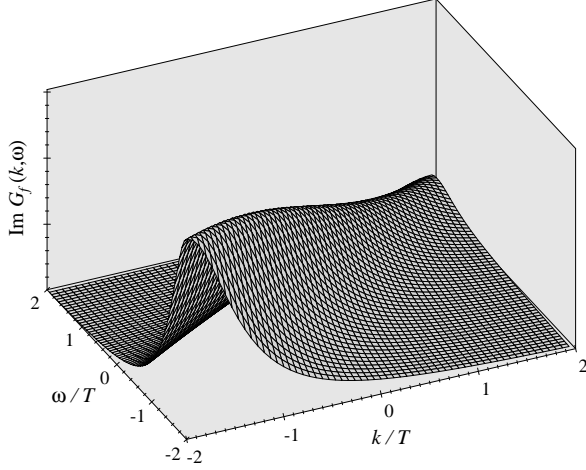


FIG. 12. Low-frequency photoemission intensity near a nodal point, $\text{Im } G_f(k, \omega) n_f(\omega)$, given by (4.1), (4.2). Here, $\Gamma_f/T = 0.58$, which is the result for the d -wave to $(s^* + id)$ -wave or $(d_{x^2-y^2} + id_{xy})$ -wave transition discussed in Sec. III A, and $n_f(\omega) = [\exp(\omega/T) + 1]^{-1}$ denotes the Fermi function.

with $|\omega|, |k| \gg T$, we obtain in addition to the leading term in (4.3), subleading T -dependent corrections $\text{Re} \tilde{\Sigma}_f^{(1)} \sim T^2/\omega$ and $\text{Im} \tilde{\Sigma}_f^{(1)} \sim T^3/\omega^2$. These are still very small contributions, and so we can expect that the system will be exceptionally sensitive to non-universal corrections to scaling right at the threshold frequency. We believe that the most important of these will come from elastic scattering off impurities; for a weak impurity scattering potential, U_{imp} , we have the additional contribution

$$\Sigma_{\text{imp}} \sim iU_{\text{imp}}^2|\omega|. \quad (4.4)$$

We have added (4.4), with a very small prefactor, to (4.3) and plotted the result in Fig. 13; the contribution of (4.4) can be neglected almost everywhere except right near the threshold.

It is interesting to note that our results (4.2) and (4.3) bear a superficial similarity to the “marginal Fermi liquid” fitting functions⁸¹. More specifically, (i) in the latter approach, the prefactor of the power of T in (4.1) is absent; (ii) the small $|\omega|/T$ behavior of the self-energy in (4.2) is similar to that of the marginal Fermi liquid; (iii) for large $|\omega|/T$, the k dependence in (4.3) (as in $\text{Im} \tilde{\Sigma} \sim |\omega - k|\theta(|\omega| - |k|)$) is replaced simply by $\text{Im} \tilde{\Sigma} \sim |\omega|$. A significance consequence of this last difference is that our large k spectral densities have more asymmetric lineshapes (even before being multiplied by the Fermi function, as is necessary for photoemission experiments), than those found in the marginal Fermi liquid functions; this is illustrated in Fig. 14. It would be interesting for experiments to test for the k dependence predicted in (4.3).

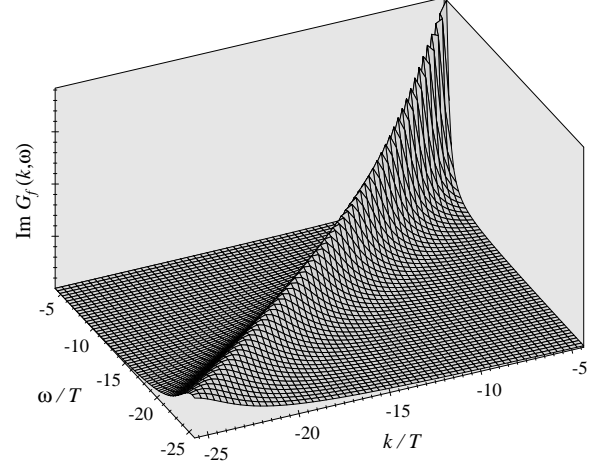


FIG. 13. High-frequency photoemission intensity near a nodal point, $\text{Im } G_f(k, \omega) n_f(\omega)$, given by (4.3), (4.4), with a small impurity contribution $U_{\text{imp}}^2 = 0.1$.

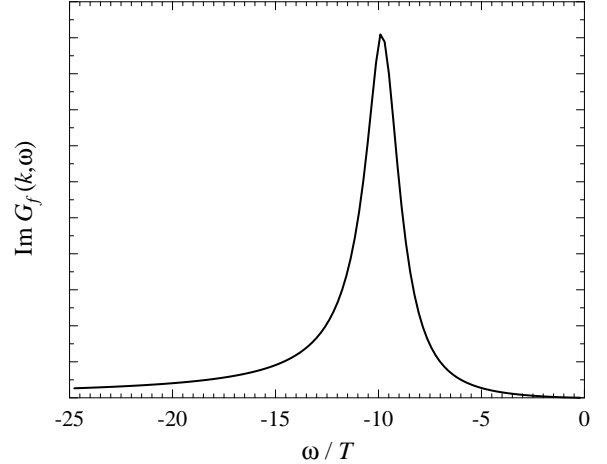


FIG. 14. Sample spectral function for $k/T = 10$ – this is a cut through the spectrum of Fig. 13. The asymmetry of the lineshape is clearly visible (and it is not simply due to the Fermi function occurring as prefactor of the photoemission intensity).

Finally, we reiterate an important feature of our analysis of quantum criticality: we have only found Lorentz-invariant fixed points at which all excitations have equal and isotropic velocities. Section III A 1 showed that, for the d -wave to $(s^* + id)$ -wave or $(d_{x^2-y^2} + id_{xy})$ -wave transition, such a fixed point was at least linearly stable to perturbations which *e.g.* set $v_F \neq v_\Delta$. However, this does not rule out the possibility that there may be other non-Lorentz-invariant fixed points of the renormalization group equations in which v_F/v_Δ is significantly different from unity. Experimentally⁴⁸, it is clear that $v_F \neq v_\Delta$, but this is still compatible with a Lorentz-invariant fixed point: we found in Section III A 1 that the leading irrelevant operator which breaks Lorentz symmetry had a scaling dimension of very small absolute value ($\epsilon/21 \approx 0.048$), and so the system can reside in a transient region with $v_F \neq v_\Delta$ over a very wide temperature range. This issue will be addressed further in future work.

Notes added: (i) Recent THz conductivity measurements on $\text{Bi}_2\text{Sr}_2\text{CaCu}_2\text{O}_{8+\delta}$ by Corson *et al.*⁸² have obtained a quasiparticle relaxation rate linearly proportional to T , at temperatures well below T_c . Combined with the photoemission experiments⁴⁰, these results provide strong support for quantum critical damping of the nodal quasiparticles in the d -wave superconductor, as is expected near a class A quantum critical point between two superconducting states. Corson *et al.* observe the quantum critical damping above 20K, which suggests that the energy per coherence volume of the second superconducting state (say, the $(d_{x^2-y^2} + id_{xy})$ superconductor) is higher than that of the d -wave superconductor by less than 20 K.

(ii) A recent work⁸³ has given a unified discussion of the quantum phase transitions considered here, and those involving \mathcal{M} symmetry breaking considered in Ref. 29.

ACKNOWLEDGMENTS

We thank L. Balents, A. Castro Neto, D. Khomskii, J. Kirtley, S. Kivelson, J. B. Marston, C. Nayak, C. M. Varma and especially P. Johnson, M. Norman, M. Randeria, and J. Zaanen for useful discussions. This research was supported by US NSF Grant No DMR 96-23181 and by the DFG (VO 794/1-1).

APPENDIX A: PERTURBATION THEORY FOR FERMION DAMPING

This appendix will compute the $T > 0$ scaling function for the fermion spectral weight in (1.1) for the case of a quantum critical point between a d -wave and a $(s^* + id)$ -wave or $(d_{x^2-y^2} + id_{xy})$ -wave superconductor. We will use a simple renormalized perturbative expansion at the fixed point found in Section III A. We will show that

such a procedure leads to spurious singularities in the low frequency regime $\hbar\omega < k_B T$. These singularities were cured by the self-consistent analysis described in Section III A 2.

From the expression (3.25), we obtain to leading order in λ^2 and ϵ

$$\begin{aligned} \left(\frac{\mu}{T}\right)^{-\eta_f} G_f^{-1}(k, \omega_n) = & (-i\omega_n + k_x \tau^z + k_y \tau^x) \left(1 - \frac{\lambda^{*2}}{2} \left(\frac{1}{\epsilon} + \ln(\mu/T)\right)\right) \\ & + \frac{\lambda^{*2}}{S_{d+1}} \int \frac{d^d p}{(2\pi)^d} T \sum_{\epsilon_n} \frac{-i\epsilon_n + p_x \tau^z + p_y \tau^x}{(p^2 + \epsilon_n^2)((k-p)^2 + (\omega_n - \epsilon_n)^2)}. \end{aligned}$$

Evaluating the frequency summation, and performing the momentum integration over the terms not involving any thermal Bose or Fermi factors, we obtain

$$\begin{aligned} \left(\frac{\mu}{T}\right)^{-\eta_f} G_f^{-1}(k, \omega_n) = & -\tilde{\Sigma}_f^{(1)}(k, \omega_n) + \\ & (-i\omega_n + k_x \tau^z + k_y \tau^x) \left(1 - \frac{\eta_f}{2} \left(\ln\left(\frac{\omega_n^2 + k^2}{eT^2}\right)\right)\right) \end{aligned} \quad (\text{A1})$$

where we have used (3.13), and $\tilde{\Sigma}_f^{(1)}$ is a thermal contribution which vanishes as $T \rightarrow 0$. To leading order in ϵ , the expression for $\tilde{\Sigma}_f^{(1)}$ can be evaluated in $d = 3$, and we obtain for k along the x direction (recall that below (3.1) we rotated the axes by 45 degrees from the axes of the square lattice):

$$\begin{aligned} \tilde{\Sigma}_f^{(1)}(k, \omega_n) = & -16\pi^2 \eta_f \int \frac{d^3 p}{(2\pi)^3} \frac{1}{2p|\mathbf{p} - \mathbf{k}|} \\ & \times \left(\frac{[n(|\mathbf{p} - \mathbf{k}|) + f(p)][p_x \tau^z (p - |\mathbf{p} - \mathbf{k}|) - i\omega_n p]}{(p - |\mathbf{p} - \mathbf{k}|)^2 + \omega_n^2} \right. \\ & \left. + \frac{[n(|\mathbf{p} - \mathbf{k}|) - f(p)][p_x \tau^z (p + |\mathbf{p} - \mathbf{k}|) - i\omega_n p]}{(p + |\mathbf{p} - \mathbf{k}|)^2 + \omega_n^2} \right) \end{aligned} \quad (\text{A2})$$

where $p = |\mathbf{p}|$, $k = |\mathbf{k}|$, $n(k)$ is the Bose function, and $f(k)$ is the Fermi function. The expression in (A2) is reliable for $|\omega|, k \gg T$: evaluating the integrals in this regime we obtain the estimates quoted below (4.3). On the contrary, for $|\omega|, k \ll T$, the above expressions are pathological; we obtain *e.g.* $\text{Im}\tilde{\Sigma}_f^{(1)}(0, \omega) \sim T^2 \delta(\omega)$. This should be contrasted with the smooth behavior as a function of ω assumed in (3.19). The latter is the correct result on physical grounds⁸⁴, and estimation of the damping constants requires a self-consistent approach like that followed in Section III A 2.

¹ J. Zaanen, *Physica C* **317**, 217 (1999).

- ² J. Tworzydło, O. Y. Osman, C. N. A. van Duin, and J. Zaanen, *Phys. Rev. B* **59**, 115 (1999).
- ³ V. J. Emery, S. A. Kivelson, and J. M. Tranquada, *Proc. Natl. Acad. Sci. USA* **96**, 8814 (1999).
- ⁴ See the review S. Sachdev, *Science* **288**, 475 (2000).
- ⁵ S. Sachdev and N. Read, *Int. J. Mod. Phys. B* **5**, 219 (1991).
- ⁶ M. Vojta and S. Sachdev, *Phys. Rev. Lett.* **83**, 3916 (1999).
- ⁷ N. Read and S. Sachdev, *Phys. Rev. Lett.* **62**, 1694 (1989); *Phys. Rev. B* **42**, 4568 (1990).
- ⁸ M. P. Gelfand, R. R. P. Singh, and D. A. Huse, *Phys. Rev. B* **40**, 10801 (1989).
- ⁹ N. Read and S. Sachdev, *Phys. Rev. Lett.* **66**, 1773 (1991).
- ¹⁰ V. N. Kotov, J. Oitmaa, O. P. Sushkov, and Zheng Weihong, *Phys. Rev. B* **60**, 14613 (1999); R. R. P. Singh, Zheng Weihong, C. J. Hamer, and J. Oitmaa, *Phys. Rev. B* **60**, 7278 (1999); V. N. Kotov and O. P. Sushkov, *Phys. Rev. B* **61**, 11820 (2000).
- ¹¹ O. P. Sushkov, cond-mat/9907400, cond-mat/0002421.
- ¹² We define the operator which creates a particle on a bond by $a_{1\alpha}^\dagger = (c_{1\alpha}^\dagger + c_{2\alpha}^\dagger)/\sqrt{2}$, where 1,2 are sites on the ends of the bond; then the bond charge density is $a^\dagger a$. Clearly, there can be no bond-charge density modulation in spin models in which the electron occupation number is constrained to be exactly unity per site. However, it appears once the connection to the operators of the parent Hubbard-like model is accounted for.
- ¹³ S. Sachdev, *Quantum Phase Transitions*, Cambridge University Press, Cambridge (1999).
- ¹⁴ I. Affleck and J. B. Marston, *Phys. Rev. B* **37**, 3774 (1988).
- ¹⁵ H. Schulz, *Phys. Rev. B* **39**, 2940 (1989).
- ¹⁶ J. B. Marston and I. Affleck, *Phys. Rev. B* **39**, 11538 (1989).
- ¹⁷ Z. Wang, G. Kotliar, X.-F. Wang, *Phys. Rev. B* **42**, 8690 (1990).
- ¹⁸ A. Nersisyan, *Phys. Lett. A* **153**, 49 (1991); A. Nersisyan, G. Japaridze, and I. Kimeridze, *J. Phys.: Condens. Matter* **3**, 3353 (1991).
- ¹⁹ S. A. Kivelson, E. Fradkin, and V. J. Emery, *Nature* **393**, 550 (1998). See also V. J. Emery, S. A. Kivelson, and O. Zachar, *Phys. Rev. B* **56**, 6120 (1997) and Ref 52.
- ²⁰ J. Zaanen and O. Gunnarsson, *Phys. Rev. B* **40**, 7391 (1989).
- ²¹ H. Schulz, *J. de Physique* **50**, 2833 (1989).
- ²² K. Machida, *Physica* **158C**, 192 (1989); M. Kato, K. Machida, H. Nakanishi, M. Fujita, *J. Phys. Soc. Jpn* **59**, 1047 (1990).
- ²³ B. I. Shraiman and E. D. Siggia, *Phys. Rev. B* **42**, 2485 (1990); S. Sachdev, *Phys. Rev. B* **49**, 6770 (1994).
- ²⁴ O. Zachar, S. A. Kivelson, and V. J. Emery, *Phys. Rev. B* **57**, 1422 (1998).
- ²⁵ J. M. Tranquada, J. D. Axe, N. Ichikawa, Y. Nakamura, S. Uchida, and B. Nachumi, *Phys. Rev. B* **54**, 7489 (1996).
- ²⁶ H. Kimura, K. Hirota, H. Matsushita, K. Yamada, Y. Endoh, S.-H. Lee, C. F. Majkrzak, R. Erwin, G. Shirane, M. Greven, Y. S. Lee, M. A. Kastner, and R. J. Birgeneau, *Phys. Rev. B* **59**, 6517 (1999).
- ²⁷ Y. S. Lee, R. J. Birgeneau, M. A. Kastner, Y. Endoh, S. Wakimoto, K. Yamada, R. W. Erwin, S.-H. Lee, and G. Shirane, *Phys. Rev. B* **60**, 3643 (1999).
- ²⁸ A. H. Castro Neto and D. Hone, *Phys. Rev. Lett.* **76**, 2165 (1996).
- ²⁹ M. Vojta, C. Buragohain, and S. Sachdev, *Phys. Rev. B* **61**, 15152 (2000).
- ³⁰ A. W. Hunt, P. M. Singer, K. R. Thurber, and T. Imai, *Phys. Rev. Lett.* **82**, 4300 (1999); T. Imai, C. P. Slichter, K. Yoshimura, and K. Kosuge, *ibid* **70**, 1002 (1993); T. Imai, C. P. Slichter, K. Yoshimura, M. Katoh, and K. Kosuge, *Phys. Rev. Lett.* **71**, 1254 (1993); S. Fujiyama, M. Takigawa, Y. Ueda, T. Suzuki, N. Yamada, *Phys. Rev. B* **60**, 9801 (1999).
- ³¹ D. K. Morr, J. Schmalian, and D. Pines, cond-mat/0002164.
- ³² G. Kotliar, *Phys. Rev. B* **37**, 3664 (1988).
- ³³ D. S. Rokhsar, *Phys. Rev. Lett.* **70**, 493 (1993).
- ³⁴ R. B. Laughlin, *Physica* **243C**, 280 (1994); R. B. Laughlin, *Phys. Rev. Lett.* **80**, 5188 (1998); A. V. Balatsky, *Phys. Rev. B* **61**, 6940 (2000); T. Maitra, cond-mat/0002114.
- ³⁵ T. Senthil, J. B. Marston, and M. P. A. Fisher, *Phys. Rev. B* **60**, 4245 (1999).
- ³⁶ S. R. White and D. J. Scalapino, *Phys. Rev. Lett.* **80**, 1272 (1998); **81**, 3227 (1998); *Phys. Rev. B* **60**, R753 (1999).
- ³⁷ C. Honerkamp, M. Salmhofer, N. Furukawa, and T. M. Rice, cond-mat/9912358.
- ³⁸ U. Ledermann, K. Le Hur, and T. M. Rice, cond-mat/0002445.
- ³⁹ B. P. Stojković, Z. G. Yu, A. R. Bishop, A. H. Castro Neto, and N. Grønbech-Jensen, *Phys. Rev. Lett.* **82**, 4679 (1999); cond-mat/9911380.
- ⁴⁰ T. Valla, A. V. Fedorov, P. D. Johnson, B. O. Wells, S. L. Hulbert, Q. Li, G. D. Gu, and N. Koshizuka, *Science* **285**, 2110 (1999).
- ⁴¹ A. V. Balatsky, P. Kumar, and J. R. Schrieffer, *Phys. Rev. Lett.* **84**, 4445 (2000). Our order parameter, ϕ , measures the amplitude oscillations of the d_{xy} component about zero amplitude at a fixed phase ($\pm\pi/2$) relative to the stable $d_{x^2-y^2}$ state, whereas Balatsky *et al.* work in the state with global $(d_{x^2-y^2} + id_{xy})$ order and consider oscillations in the relative phase between the two components, both of which have a non-zero amplitude. The frequency of the amplitude oscillations we consider vanishes at the critical point between the two superconductors. Also, the susceptibility corresponding to this amplitude mode will diverge at this critical point.
- ⁴² K. Krishana, N. P. Ong, Q. Li, G. D. Gu, and N. Koshizuka, *Science* **277**, 83 (1997); H. Aubin, K. Behnia, S. Ooi, and T. Tamegai, *Phys. Rev. Lett.* **82**, 624 (1999).
- ⁴³ L. Balents, M. P. A. Fisher, and C. Nayak, *Int. J. Mod. Phys. B* **12**, 1033 (1998).
- ⁴⁴ C. Castellani, C. di Castro, and M. Grilli, *Phys. Rev. Lett.* **75**, 4650 (1995), *Z. Phys. B* **103**, 137 (1997), *J. Phys. Chem. Solids* **59**, 1694 (1998).
- ⁴⁵ Z.-X. Shen and D. S. Dessau, *Phys. Rep.* **253**, 1 (1995).
- ⁴⁶ J. C. Campuzano *et al.*, in *The Gap Symmetry and Fluctuations in High- T_c Superconductors*, eds. J. Bok *et al.* (Plenum, New York, 1998), p. 229.
- ⁴⁷ A. V. Fedorov, T. Valla, P. D. Johnson, Q. Li, G. D. Gu, and N. Koshizuka, *Phys. Rev. Lett.* **82**, 2179 (1999).
- ⁴⁸ J. Mesot, M. R. Norman, H. Ding, M. Randeria, J. C. Campuzano, A. Paramekanti, H. M. Fretwell, A. Kaminiski, T. Takeuchi, T. Yokoya, T. Sato, T. Takahashi,

- T. Mochiku, and K. Kadowaki, Phys. Rev. Lett. **83**, 840 (1999).
- ⁴⁹ A. Kaminski, J. Mesot, H. Fretwell, J. C. Campuzano, M. R. Norman, M. Randeria, H. Ding, T. Sato, T. Takahashi, T. Mochiku, K. Kadowaki, and H. Hoechst, Phys. Rev. Lett. **84**, 1788 (2000).
- ⁵⁰ F. Tafuri and J. R. Kirtley, cond-mat/0003106.
- ⁵¹ D. B. Bailey, M. Sigrist, and R. B. Laughlin, Phys. Rev. B **55**, 15239 (1997); M. Sigrist, Prog. Theor. Phys. **99**, 899 (1998).
- ⁵² V. J. Emery, S. A. Kivelson, and H. Q. Lin, Phys. Rev. Lett. **64**, 475 (1990); Phys. Rev. B **42**, 6523 (1990).
- ⁵³ S. A. Kivelson and V. J. Emery in *Strongly Correlated Electronic Materials: The Los Alamos Symposium 1993*, edited by K.S. Bedell, Z. Wang, D.E. Meltzer, A.V. Balatsky, and E. Abrahams, (Addison-Wesley, Reading, Massachusetts, 1994) p. 619.
- ⁵⁴ U. Löw, V. J. Emery, K. Fabricius, and S. A. Kivelson, Phys. Rev. Lett. **72**, 1918 (1994).
- ⁵⁵ C. Hellberg and E. Manousakis, Phys. Rev. Lett. **78**, 4069 (1997).
- ⁵⁶ S. Sachdev, Phys. Rev. B **45**, 12377 (1992).
- ⁵⁷ S. Sachdev and Z. Wang, Phys. Rev. B **43**, 10229 (1991).
- ⁵⁸ D. Foerster, cond-mat/0001385.
- ⁵⁹ N. Read and S. Sachdev, Nucl. Phys. B **316**, 609 (1989); D. Rokhsar, Phys. Rev. B **42**, 2526 (1990).
- ⁶⁰ M. Grilli, C. Castellani, and G. Kotliar, Phys. Rev. B **45**, 10805 (1992).
- ⁶¹ In our earlier work⁶ we had implicitly assumed a cut-off or exponential decay of V_{ij} for large distances. Doing so, the “striped” states survive down to $\delta \rightarrow 0$, and the relation $p \sim 1/\delta$ is exact in this limit.
- ⁶² J. M. Tranquada, J. Phys. Chem. Solids **59**, 2150 (1998).
- ⁶³ S. Wakimoto, R. J. Birgeneau, Y. Endoh, P. M. Gehring, K. Hirota, M. A. Kastner, S. H. Lee, Y. S. Lee, G. Shirane, S. Ueki, and K. Yamada, Phys. Rev. B **60**, R769 (1999); S. Wakimoto, K. Yamada, S. Ueki, G. Shirane, Y. S. Lee, S. H. Lee, M. A. Kastner, K. Hirota, P. M. Gehring, Y. Endoh, R. J. Birgeneau, J. Phys. Chem. Solids **60**, 1079 (1999).
- ⁶⁴ H.-H. Lin, L. Balents, and M. P. A. Fisher, Phys. Rev. B **56**, 6569 (1997).
- ⁶⁵ N. Ichikawa, S. Uchida, J. M. Tranquada, T. Niemoeller, P. M. Gehring, S.-H. Lee, and J. R. Schneider, cond-mat/9910037.
- ⁶⁶ G. B. Teitelbaum, B. Büchner, and H. de Gronckel, Phys. Rev. Lett. **84**, 2949 (2000).
- ⁶⁷ J. B. Marston, cond-mat/9904437, proceedings of *The International Workshop on Superconductivity, Magneto-Resistive Materials, and Strongly Correlated Systems*, Hanoi, Vietnam, January 1999 (to appear).
- ⁶⁸ D. A. Ivanov, P. A. Lee, X.-G. Wen, Phys. Rev. Lett. **84**, 3958 (2000); X. G. Wen and P. A. Lee, Phys. Rev. Lett. **76**, 503 (1996); P. A. Lee, N. Nagaosa, T. K. Ng, X.-G. Wen, Phys. Rev. B **57**, 6003 (1998).
- ⁶⁹ C. Nayak, cond-mat/0001303; cond-mat/0001428.
- ⁷⁰ B. G. Kotliar and J. Liu, Phys. Rev. B **38**, 5142 (1988).
- ⁷¹ E. Cappelluti and R. Zeyer, Phys. Rev. B **59**, 6475 (1999).
- ⁷² J. B. Marston and C.-H. Chung, to be published.
- ⁷³ D.-H. Lee, Phys. Rev. B **60**, 12429 (1999).
- ⁷⁴ J. Zinn-Justin, *Quantum Field Theory and Critical Phenomena*, Clarendon Press, Oxford (1993), Section 10.8.
- ⁷⁵ S. Sachdev, Phys. Rev. B **55**, 142 (1997); Phys. Rev. B **59**, 14054 (1999).
- ⁷⁶ In Ref 13 a more general fitting function was used for G_b , equivalent to the form $G_b^{-1} \propto (\alpha^2 k^2 - \omega^2 - i\omega\omega_1 + \omega_2^2)$; a very good best-fit to the exact result was found for $\alpha = 1.02$ and $\omega_2 = 2.01\omega_1$ (see Eqn (4.116) in Ref 13). The form in (3.19) is equivalent to assuming $\alpha = 1$ and $\omega_2 = 2\omega_1$, which are clearly excellent approximations.
- ⁷⁷ E. Brézin, J. C. Le Guillou, J. Zinn-Justin in *Phase Transitions and Critical Phenomena*, **6**, C. Domb and M. S. Green eds, Academic Press, London (1976).
- ⁷⁸ G. Baskaran, Z. Zou, and P. W. Anderson, Solid State Commun. **63**, 973 (1987); A. E. Ruckenstein, P. J. Hirschfeld, and J. Appel, Phys. Rev. B **36**, 857 (1987).
- ⁷⁹ C. M. Varma, Phys. Rev. B **55**, 14554 (1997); Phys. Rev. Lett. **83**, 3538 (1999); Phys. Rev. B **61**, R3804 (2000).
- ⁸⁰ V. P. Gusynin, V. M. Loktev, and S. G. Sharapov, Sov. Phys. JETP **90**, 993 (2000); M. Franz and A. J. Millis, Phys. Rev. B **58**, 14572 (1998); H.-J. Kohn and A. T. Dorsey, Phys. Rev. B **59**, 6438 (1999).
- ⁸¹ C. M. Varma, P. B. Littlewood, S. Schmitt-Rink and A. E. Ruckenstein, Phys. Rev. Lett. **63**, 1996 (1989); E. Abrahams and C. M. Varma, Proc. Natl. Acad. Sci. USA **97**, 5714 (2000).
- ⁸² J. Corson, J. Orenstein, and J. N. Eckstein, cond-mat/0003243.
- ⁸³ S. Sachdev and M. Vojta, cond-mat/0005250.
- ⁸⁴ S. Sachdev and J. Ye, Phys. Rev. Lett. **69**, 2411 (1992).